

RESEARCH ARTICLE

ACSL3 is a novel GABARAPL2 interactor that links ufmylation and lipid droplet biogenesis

Franziska Eck¹, Santosh Phuyal², Matthew D. Smith³, Manuel Kaulich⁴, Simon Wilkinson³, Hesso Farhan² and Christian Behrends^{1,*}

ABSTRACT

While studies of the autophagy-related (ATG) genes in knockout models have led to an explosion of knowledge about the functions of autophagy components, the exact roles of LC3 and GABARAP family proteins (human ATG8 equivalents) are still poorly understood. A major drawback in understanding their roles is that the available interactome data has largely been acquired using overexpression systems. To overcome these limitations, we employed CRISPR/Cas9-based genome-editing to generate a panel of cells in which human ATG8 genes were tagged at their natural chromosomal locations with an N-terminal affinity epitope. This cellular resource was employed to map endogenous GABARAPL2 protein complexes using interaction proteomics. This approach identified the ER-associated protein and lipid droplet (LD) biogenesis factor ACSL3 as a stabilizing GABARAPL2-binding partner. GABARAPL2 bound ACSL3 in a manner dependent on its LC3-interacting regions, whose binding site in GABARAPL2 was required to recruit the latter to the ER. Through this interaction, the UFM1-activating enzyme UBA5 became anchored at the ER. Furthermore, ACSL3 depletion and LD induction affected the abundance of several ufmylation components and ER-phagy. Together these data allow us to define ACSL3 as a novel regulator of the enigmatic UFM1 conjugation pathway.

KEY WORDS: GABARAPL2, ACSL3, Lipid droplets, UBA5, Ufmylation, ER-phagy

INTRODUCTION

From yeast to humans, ATG8s are highly conserved proteins. While there is only a single Atg8 in yeast, the human ATG8 (hATG8) family is subdivided into the orthologs of the microtubule-associated protein 1A/1B light chain 3 (MAP1LC3) family, comprising LC3A, LC3B and LC3C, and the γ -aminobutyric acid receptor-associated protein (GABARAP) family, comprising GABARAP, GABARAPL1 and GABARAPL2 (Slobodkin and Elazar, 2013). All six hATG8 proteins share the same ubiquitin-like fold, although they do not exhibit any sequence similarities with ubiquitin. However, within and between the ATG8 subfamily

members, the amino acid sequences show high similarities (Shpilka et al., 2011). A major feature of LC3 and GABARAP proteins is their covalent conjugation to the phospholipid phosphatidylethanolamine (PE). This process is initiated by the cysteine proteases ATG4A–ATG4D, which cleave all hATG8 family members to expose a C-terminal glycine residue, and is followed by the activation of LC3s and GABARAPs through the E1-like activating enzyme ATG7. PE conjugation of hATG8 proteins is subsequently accomplished in a concerted action of the E2-like conjugating enzyme ATG3 and the E3-like ligase scaffold complex ATG12–ATG5–ATG16L1. PE–hATG8 conjugation is reversible through cleavage by ATG4A–ATG4D (Mizushima et al., 2011).

The best understood function of hATG8s is in macroautophagy (hereafter referred to as autophagy), which is a highly conserved degradation pathway that eliminates defective and unneeded cytosolic material and is rapidly upregulated by environmental stresses, such as nutrient deprivation. In the past years, it has been shown that autophagy is capable of selectively recognizing and engulfing diverse cargo, such as aggregated proteins (aggrephagy), pathogens (xenophagy) or mitochondria (mitophagy) with the help of specific receptor proteins (Kirkin and Rogov, 2019). Initiation of autophagy leads to the formation of phagophores (also called isolation membranes) from preexisting membrane compartments, such as the ER. Elongation and closure of isolation membranes leads to engulfment of cargo inside double membrane vesicles termed autophagosomes. Fusion of autophagosomes with lysosomes forms autolysosomes, in which captured cargo is degraded in bulk by lysosomal hydrolases (Dikic and Elazar, 2018). During this process, GABARAPs and LC3s are associated with the outer and inner membrane of phagophores and regulate membrane expansion (Xie et al., 2008), cargo receptor recruitment (Stolz et al., 2014), closure of phagophores (Weidberg et al., 2011) and the fusion of autophagosomes with lysosomes (Nguyen et al., 2016).

Besides autophagy, GABARAPs and LC3s are implicated in a number of other cellular pathways. For example, GABARAP was initially identified as an interactor of the GABA receptor and is involved in its intracellular transport to the plasma membrane (Leil et al., 2004; Wang et al., 1999), while GABARAPL2 was identified as modulator of Golgi reassembly and intra-Golgi trafficking (Legesse-Miller et al., 1998; Müller et al., 2002). GABARAPs have also been shown to be essential scaffolds for the ubiquitin ligase CUL3^{KBTBD6/KBTBD7} (Genau et al., 2015). Among other functions, LC3s have regulatory functions in RhoA-dependent actin cytoskeleton reorganization (Baisamy et al., 2009) as well as in the regulation of ER exit sites (ERES) and COPII-dependent ER-to-Golgi transport (Stadel et al., 2015). This high functional diversity of GABARAPs and LC3s implies that these proteins are more than autophagy pathway components, and that there are possible other unique functions of individual hATG8 proteins to be unraveled.

¹Munich Cluster for Systems Neurology (SyNergy), Medical Faculty, Ludwig-Maximilians-University München, Feodor-Lynen Strasse 17, 81377 Munich, Germany. ²Institute of Basic Medical Sciences, Department of Molecular Medicine, University of Oslo, Sognsvannsveien 9, 0372 Oslo, Norway. ³Cancer Research UK Edinburgh Centre, MRC Institute of Genetics and Molecular Medicine, University of Edinburgh, Edinburgh EH4 2XR, UK. ⁴Institute of Biochemistry II, Goethe University School of Medicine, Theodor-Stern-Kai 7, 60590 Frankfurt am Main, Germany.

*Author for correspondence (christian.behrends@mail03.med.uni-muenchen.de)

DOI: 10.1242/jcs.243477; M.D.S., 0000-0001-7603-8628; M.K., 0000-0002-9528-8822; C.B., 0000-0002-9184-7607

Handling Editor: John Heath

Received 1 January 2020; Accepted 10 August 2020

So far, interactome and functional analyses of LC3s and GABARAPs have been mostly performed in cells overexpressing one of the six hATG8 family members (Behrends et al., 2010; Popovic et al., 2012). This raises the concern that an overexpressed hATG8 protein might take over functions or interactions of one of the other family members due to their high sequential and structural similarity. A lack of isoform-specific antibodies further complicates the analysis of distinct functions of hATG8s. To facilitate the study of endogenous GABARAPs and LC3s, it is important to generate alternative resources and tools, such as multiple hATG8 knockout cell lines (Nguyen et al., 2016) or hATG8 family member-specific peptide sensors (Stolz et al., 2017). To circumvent the hATG8 antibody problem, here, we used CRISPR/Cas9 technology to seamlessly tag hATG8 genes at their natural chromosomal locations. The generated cell lines (hATG8^{endoHA}) express N-terminally hemagglutinin (HA)-tagged hATG8 family members at endogenous levels and are a powerful tool to study the functions of individual GABARAPs and LC3s. All created cell lines were tested for their correct sequence and functionality. As a proof of concept, we performed interaction proteomics with the GABARAPL2^{endoHA} cell line and characterized the interaction with the novel binding partner ACSL3.

RESULTS

Establishment of cells carrying endogenously HA-tagged LC3s and GABARAPs

As complementary cell lines to our previously reported LC3C^{endoHA} HeLa cell line (Le Guerroué et al., 2017), we sought to employ CRISPR-mediated gene-editing to generate a panel of cells in which the remaining five hATG8 family members are seamlessly epitope tagged at their natural chromosomal locations. To this end, we directed Cas9 to cleave DNA at the vicinity of the start codon of the LC3 and GABARAP genes in order to stimulate microhomology-mediated integration of a sequence encoding for a single HA tag using a double-stranded DNA donor molecule containing short homology arms (Kaulich and Dowdy, 2015). Briefly, we designed PCR homology templates in which a blasticidine-resistant gene, a P2A sequence and the open reading frame of the HA tag were flanked by homology arms to the 5'UTRs and first exons of the LC3/GABARAP genes (Fig. S1A). In parallel, we designed single guide RNAs (sgRNAs) for all hATG8 genes except LC3C and cloned them into pX330, a SpCas9-expressing vector (Fig. S1A). We then transfected HeLa cells with corresponding pairs of homology template and sgRNA for each LC3/GABARAP gene. After selection with blasticidine, single cell clones were SANGER sequenced to confirm seamless and locus-specific genomic insertion of the HA tag. While we obtained correct clones for GABARAP, GABARAPL1, GABARAPL2 and LC3B (Fig. S1B), cells that received the homology template and sgRNA for LC3A did not survive the antibiotic selection. We assume that this is due to the lack of LC3A in HeLa cells, as it has been reported that LC3A expression is suppressed in many tumor cell lines (Bai et al., 2012). Immunoblot analysis of the sequence-validated clones and the parental cells revealed the presence of the HA tag in the engineered cell lines that corresponded to the size of the tagged LC3/GABARAP protein (Fig. 1A; Fig. S2A–C). Gene-specific CRISPR/Cas9-editing was further confirmed by siRNA-mediated depletion of endogenous LC3 or GABARAP proteins in the corresponding HA-tagged hATG8 cell lines (Fig. 1B; Fig. S2D–F). Consistent with this, confocal microscopy of GABARAPL2^{endoHA} cells showed a substantially decreased HA immunolabeling upon knockdown of GABARAPL2 (Fig. 1C). Next, we examined the

integrity of the tagged LC3/GABARAP proteins by monitoring their conjugation to PE in response to treatment with small-molecule inhibitors that increase lipidation (Torin1), block autophagosomal degradation (Bafilomycin A1; BafA1) or prevent ATG8–PE conjugate formation (ATG7 inhibitor). As expected, GABARAPL2^{endoHA}, GABARAP^{endoHA} and LC3B^{endoHA} cell lines showed treatment-specific lipidation levels of the respective tagged hATG8 protein (Fig. 1D; Fig. S2G,I). We also detected lipidated GABARAPL1, although in a manner that was independent of induction or blockage of autophagy (see Fig. 3E). However, as expected, autophagy induction robustly decreased HA–GABARAPL1 protein levels in GABARAPL1^{endoHA} cells, while blockage of autophagosomal degradation led to the opposite phenotype (Fig. S2H). Next, we analyzed the subcellular distribution of one of the HA-tagged hATG8 proteins (i.e. GABARAPL2) in basal and autophagy-modulating conditions using confocal microscopy. In GABARAPL2^{endoHA} cells, HA–GABARAPL2 was indeed found to colocalize with the autophagosomal and lysosomal markers p62 (also known as SQSTM1), LC3B and LAMP1 and this colocalization increased upon combination treatment with Torin1 and BafA1 (Fig. 1E–G). Together, we successfully engineered cell lines to carry epitope-tagged hATG8 family members which retain their functionality.

Mapping the endogenous GABARAPL2 interactome

Next, we selected GABARAPL2^{endoHA} cells for a proof-of-principle immunoprecipitation (IP) followed by mass spectrometric (MS) analysis to identify new candidate binding partners of a hATG8 family member at endogenous levels. To distinguish between candidates that bind preferentially to PE-conjugated versus unconjugated GABARAPL2, we treated stable isotope labeling with amino acids in cell culture (SILAC)-labeled GABARAPL2^{endoHA} cells with Torin1 and BafA1 (light) or ATG7 inhibitor (heavy). Equal amounts of heavy and light SILAC cells were mixed, lysed and subjected to an HA IP. Immune complexes were eluted and size separated by gel electrophoresis followed by in-gel tryptic digest, peptide extraction and desalting prior to analysis by liquid chromatography tandem MS. SILAC-labeled parental HeLa cells differentially treated with Torin1 and BafA1, or ATG7 inhibitor served as a negative control. In duplicate experiments, we identified a total of 168 proteins whose abundances in GABARAPL2 immunoprecipitates were altered by at least 2.8-fold (log₂ SILAC ratio ≥1.5 or ≤−1.5) in response to modulation of the GABARAPL2 conjugation status (Fig. 2A). Among these regulated proteins were well-characterized hATG8-binding proteins such as ATG7, CCPG1 and p62, as well as several candidate interactors of LC3 and GABARAP proteins previously found in large-scale screening efforts, such as the mitochondrial outer membrane protein VDAC1, the nucleoprotein AHNK2, the translation initiation factor EIF4G1 and the small GTPase IRGQ (Ewing et al., 2007; Rolland et al., 2014) (Fig. 2A). In addition, a number of known hATG8-binding proteins, including UBA5, HADHA, HADHB, RB1CC1, TRIM21 and IPO5 was found to bind GABARAPL2 independently of its lipidation status, since these proteins did not display substantial changes in their SILAC ratios.

ACSL3 is a novel binding partner of GABARAPL2

Since functional annotation analysis of the above proteins using the DAVID tool revealed the gene ontology (GO) term 'fatty acid metabolism' (Fig. S2J), and this term had not been previously associated with LC3/GABARAP-interacting proteins, we focused

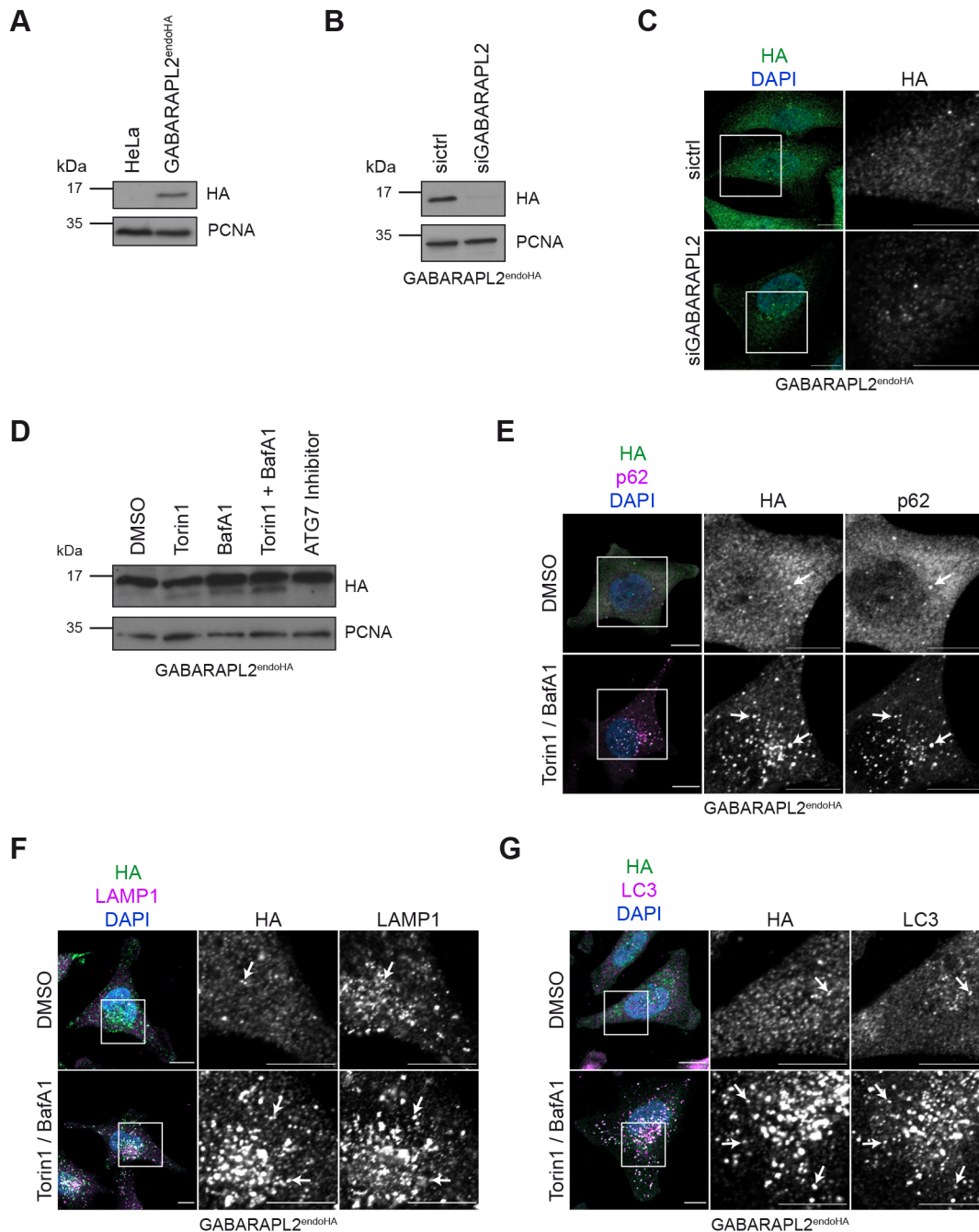


Fig. 1. Establishment of cells carrying endogenously HA-tagged LC3s and GABARAPs. (A) GABARAPL2^{endoHA} and parental HeLa cell lysates were analyzed by immunoblotting using anti-HA and -PCNA antibodies. The latter was used as loading control. (B,C) GABARAPL2^{endoHA} cells were reversely transfected for 72 h with non-targeting (siCtrl) or GABARAPL2 siRNA (siGABARAPL2) followed by lysis and immunoblot analysis (B) or fixation and immunolabeling (C) using an anti-HA antibody. (D) GABARAPL2^{endoHA} cells were treated as indicated and subjected to lysis and immunoblotting. (E–G) GABARAPL2^{endoHA} cells treated with indicated inhibitors were immunolabeled with anti-p62 (E), anti-LAMP1 (F) or anti-LC3 (G) antibodies. Arrows indicate colocalization events. Scale bars: 10 μ m.

on the proteins found in this category. In particular, the long-chain-fatty-acid-CoA ligase 3 (ACSL3) attracted our attention as it was the only ER-localized protein among these candidates. To validate ACSL3 as novel GABARAPL2-interacting protein, we performed HA IPs on lysates derived from parental and GABARAPL2^{endoHA} cells that were transiently transfected with ACSL3–Myc, Myc–p62 or Myc–ATG7 or left untreated. Notably, p62 and ATG7 served as positive controls. Immunoblotting with epitope tag- and gene-specific antibodies revealed that overexpressed and endogenous p62

and ATG7, as well as ACSL3, associated with endogenous GABARAPL2 (Fig. 2B,C). Thus, these results indicate that our hATG8^{endoHA} cells are indeed valuable tools to examine the LC3 and GABARAP interactome at endogenous protein expression levels and to identify novel binding partners such as ACSL3.

GABARAPL2 is stabilized by ACSL3

Since GABARAPL2 is involved in autophagic cargo engulfment (Schaaf et al., 2016), we tested whether ACSL3 is an autophagy

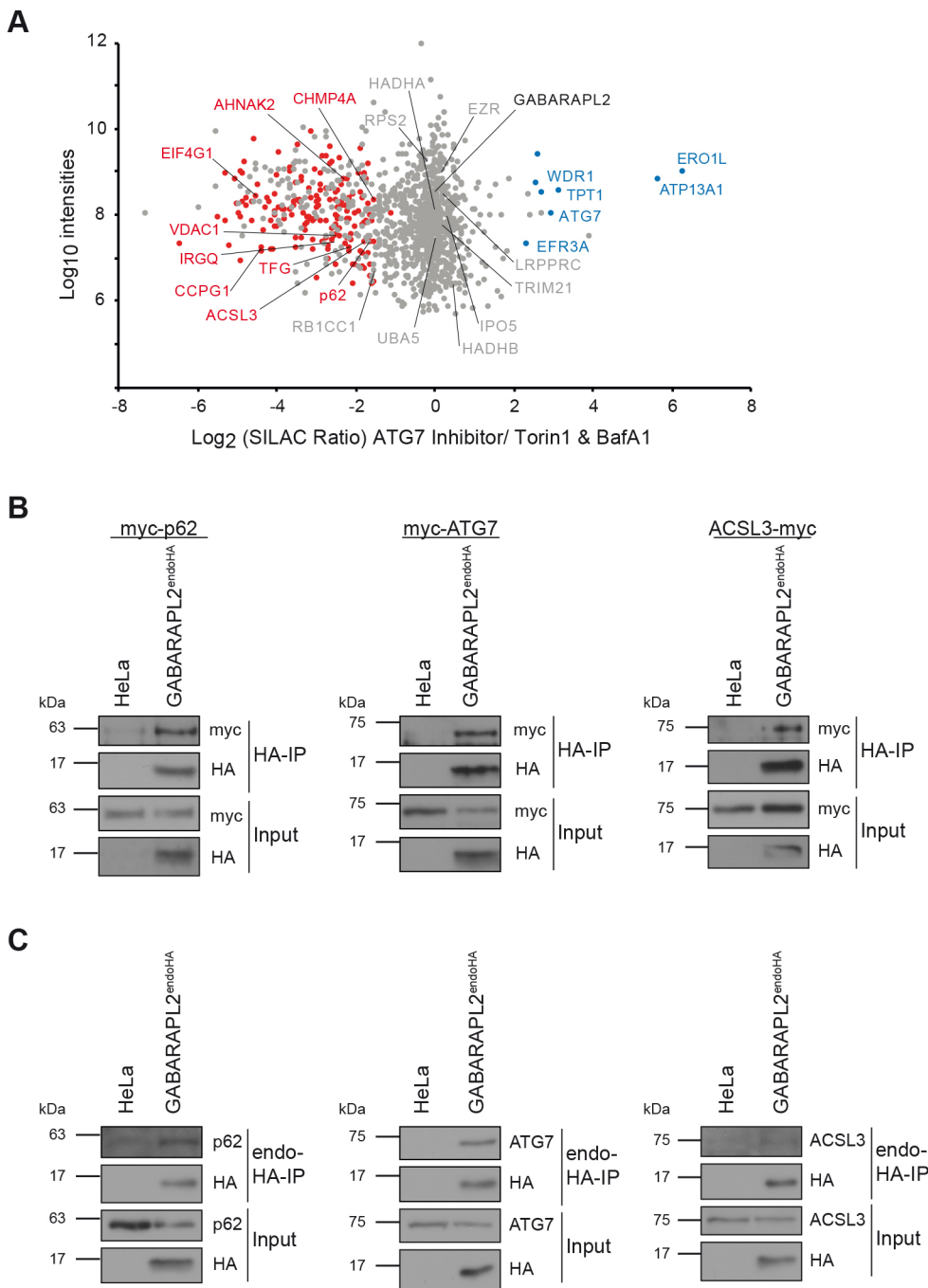


Fig. 2. Endogenous GABARAPL2 interactome. (A) Scatterplot represents interaction proteomics of SILAC-labeled GABARAPL2^{endoHA} cells differentially treated with Torin1 and BafA1 (light) or ATG7 inhibitor (heavy). Significantly enriched proteins upon Torin1 and BafA1 combination treatment or ATG7 inhibition are highlighted in red and blue, respectively. Proteins in gray are unchanged. (B,C) Immunoblot analysis of anti-HA immunoprecipitates from lysates derived from parental HeLa and GABARAPL2^{endoHA} cells which were either transiently transfected for 48 h with Myc-tagged ATG7, p62 or ACSL3 (B) or left untreated (C).

substrate or serves as a selective autophagy receptor. However, stimulation of GABARAPL2^{endoHA} cells with Torin1, BafA1, a combination of both or with ATG7 inhibitor showed that ACSL3 protein levels did not change upon autophagy induction or blockage (Fig. 3A). Likewise, depletion of GABARAPL2 had no effects on ACSL3 abundance (Fig. 3B). Thus, these results indicate that ACSL3 is neither a substrate nor a receptor of autophagy under these conditions. Next, we examined the effects of ACSL3 knockdown on GABARAPL2. Treatment of GABARAPL2^{endoHA} cells with two different ACSL3 siRNAs showed a significant decrease of GABARAPL2 protein levels (Fig. 3C). To rule out that this phenotype is due to a global perturbation of the ER, we probed for the integrity of this organelle in cells depleted of ACSL3 using immunolabeling with calnexin and the ER exit site marker SEC13.

However, neither the meshwork appearance nor the exit sites of the ER showed any overt alterations (Fig. S3A,B). Given the high structural and functional similarity between LC3 and GABARAP family members, we addressed whether ACSL3 depletion likewise impacts on the protein abundance of the other hATG8 family members. Unexpectedly, ACSL3 knockdown experiments in GABARAP^{endoHA}, GABARAPL1^{endoHA} and LC3B^{endoHA} cells did not show any significant reduction in the respective HA-tagged hATG8 proteins (Fig. 3D–F). In contrast, we found that LC3B protein levels significantly increased upon ACSL3 depletion (Fig. 3F), suggesting that reduced GABARAPL2 levels might be compensated for by increased expression of LC3B. Intriguingly, we observed that GABARAPL2 protein levels are restored in GABARAPL2^{endoHA} cells treated with ACSL3 siRNA and with

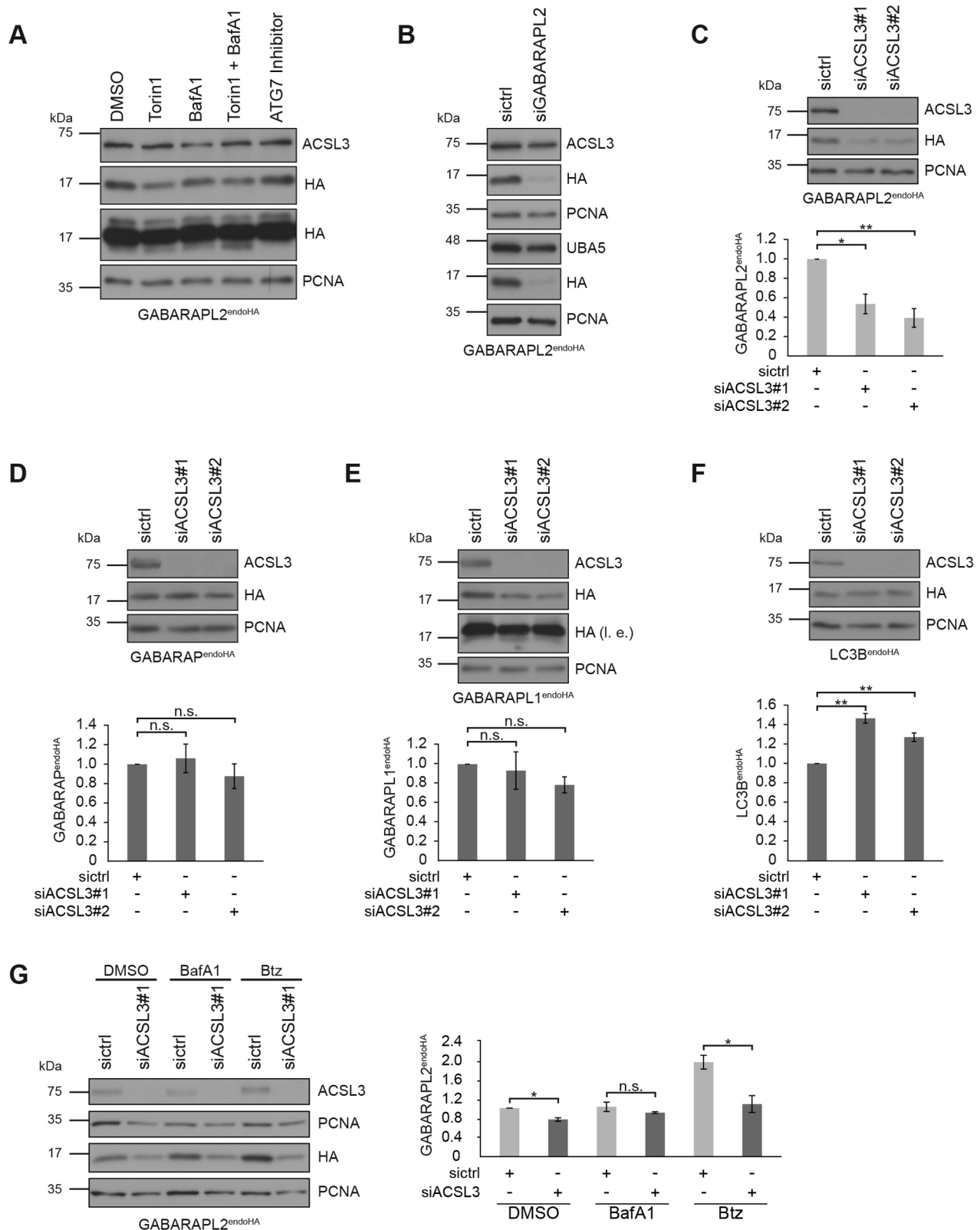


Fig. 3. Stabilization of GABARAPL2 through ACSL3. (A) GABARAPL2^{endoHA} cells were treated as indicated and subjected to lysis and analyzed with immunoblotting and anti-ACSL3 antibody. (B) Reversely transfected GABARAPL2^{endoHA} cells with non-targeting (siCtrl) or GABARAPL2 siRNA (siGABARAPL2) were lysed followed by immunoblotting and analysis with indicated antibodies. (C–F) GABARAPL2^{endoHA} (C), GABARAP^{endoHA} (D), GABARAPL1^{endoHA} (E) and LC3B^{endoHA} (F) cells were reversely transfected with two different ACSL3 siRNAs. Lysates were analyzed by immunoblotting with indicated antibodies. Data represent mean±s.e.m. Statistical analysis ($n=4$) of the HA:PCNA ratio, normalized to siCtrl, was performed using Student's t -test ($*P<0.05$, $**P<0.01$). I.e., long exposure. (G) GABARAPL2^{endoHA} cells reversely transfected with siRNAs targeting ACSL3 for 72 h were treated with BafA1 or Btz and analyzed by immunoblotting. Data represents mean±s.e.m. Statistical analysis ($n=3$) of the HA:PCNA ratio, normalized to siCtrl-DMSO, was performed using Student's t -test ($*P<0.05$). n.s., not significant.

BafA1, to block autophagosomal degradation, but not in these cells treated with the proteasome inhibitor Bortezomib (Btz) (Fig. 3G). Together, these results indicate that ACSL3 is not degraded by autophagy but rather serves as a specific stabilizing factor of GABARAPL2 at the ER.

GABARAPL2 localizes with ACSL3 at the ER

ACSL3 is one of five acyl-CoA synthetases and catalyzes the conjugation of CoA to long chain fatty acids to form acyl-CoA (Soupe and Kuypers, 2008). In addition, ACSL3 has been shown to regulate the formation, the size and the copy number of lipid droplets (LDs) (Fujimoto et al., 2007; Kassan et al., 2013). Consistent with its cellular role, ACSL3 is inserted with its N-terminal helix region midway into the lipid bilayer of the ER membrane or integrated into the monolayer of LDs, while its C-terminal part, encompassing the AMP-binding domain, is facing the cytoplasm (Brasaele et al., 2004; Ingelmo-Torres et al., 2009; Poppelreuther et al., 2012). To further validate the GABARAPL2–ACSL3 interaction, we sought to examine the subcellular localization of both proteins by confocal microscopy. However, as there were no suitable antibodies for immunofluorescence staining of endogenous ACSL3, we gene-edited GABARAPL2^{endoHA} cells to express ACSL3 tagged at its C-terminus with NeonGreen (Fig. S1A,C). Immunoblot analysis of these newly established GABARAPL2^{endoHA}/ACSL3^{endoNeonGreen} cells in comparison with GABARAPL2^{endoHA} and parental HeLa cells transfected with TOMM20–NeonGreen confirmed the correct size of the ACSL3–NeonGreen fusion (~106 kDa; ACSL3 at 80 kDa plus NeonGreen at 26 kDa) (Fig. 4A). Colocalization of ACSL3–NeonGreen with the ER-membrane-localized chaperone calnexin demonstrated that the NeonGreen tag did not interfere with the ER localization of ACSL3 (Fig. 4B). As ACSL3 is essential for LD formation, we tested whether the ACSL3–NeonGreen chimera is fully functional. For this, GABARAPL2^{endoHA}/ACSL3^{endoNeonGreen} cells were treated with oleic acid, to induce LD formation, or ethanol, as a control, prior to fixation and labeling of phospholipids and neutral lipids. Confocal microscopy showed a clear colocalization of ACSL3 with phospholipids and neutral lipids in control cells, while ACSL3 redistributed in the phospholipid monolayer of LDs when cells were treated with oleic acid for 24 h (Fig. 4C). Next, we analyzed fixed and HA-immunolabeled GABARAPL2^{endoHA}/ACSL3^{endoNeonGreen} cells by confocal microscopy and super-resolution radial fluctuations (SRRF) imaging. Consistent with our biochemical experiment, we observed partial colocalization of endogenous GABARAPL2 and ACSL3 (Fig. 4D). Together, these results show that NeonGreen-tagged ACSL3 is correctly localized at the ER membrane, integrates into the monolayer of LDs upon free fatty acid treatment and associates with GABARAPL2 at the ER.

ACSL3 binds GABARAPL2 in a LIR-dependent manner

Interaction between hATG8 proteins and their binding partners involves an ATG8 family-interacting motif [AIM; also known as the LC3-interacting region (LIR)] in the hATG8 interactors and the LIR-docking site (LDS) in LC3 and GABARAP proteins (Noda et al., 2008; Pankiv et al., 2007; Rogov et al., 2014). Amino acid sequence analysis of ACSL3 with iLIR (Kalvari et al., 2014) and manual inspection revealed that it had four potential LIRs (LIR-1, 65–71; LIR-2, 135–140; LIR-3, 589–594; LIR-4, 643–648) (Fig. 5A). To determine whether ACSL3 employs at least one of these sites to bind GABARAPL2, we performed binding experiments with purified GST-tagged wild-type and a LIR-

binding deficient GABARAPL2 mutant in which the relevant amino acids of the LDS were replaced with alanine (i.e. Y49A/L50A). These two GABARAPL2 variants were incubated with lysates derived from HeLa cells stably expressing full-length ACSL3 or two fragments thereof. While the first fragment spanned residues 1–85 and included the ER membrane-binding domain and LIR-1, the second fragment ranged from residues 86–718 and contained the AMP-binding site and LIR-2, -3 and -4 (Fig. 5A). Immunoblot analysis of the pulldown assay showed binding of wild-type GABARAPL2 to full-length ACSL3 and both of its fragments (Fig. 5B), indicating that ACSL3 contains at least two distinct binding sites for GABARAPL2. Intriguingly, GABARAPL2 lacking a functional LDS did not interact with ACSL3 86–718 while it retained binding to the wild-type ACSL3 and fragment 1–85 (Fig. 5B). This suggests that GABARAPL2 employs its LDS to bind to a LIR within residues 86–718 of ACSL3 while GABARAPL2 seem to employ a different binding site to interact with a motif in the preceding ACSL3 sequence. To start dissecting the relevance of our binding model for the recruitment of GABARAPL2 to ACSL3 at the ER, we subjected HeLa cells stably expressing wild-type or LIR-binding-deficient GABARAPL2 to subcellular fractionation using differential centrifugation. Consistent with our finding that ACSL3 binds GABARAPL2 in a LIR-dependent manner, immunoblot analysis revealed that wild-type GABARAPL2 is found in the ER fraction but GABARAPL2 Δ LDS fails to co-fractionate with the ER (Fig. 5C; Fig. S4B). Taken together, these results indicate that the ACSL3–GABARAPL2 interaction involves more than one binding motif and binding site in GABARAPL2 and ACSL3, and that LIR-dependent ACSL3 binding is required for the ER recruitment of GABARAPL2.

ACSL3 anchors UBA5 to the ER membrane

To better understand the biological significance of the GABARAPL2–ACSL3 interaction, we turned our attention to known GABARAPL2-binding proteins and in particular to the ubiquitin-like modifier activating enzyme 5 (UBA5) (Komatsu et al., 2004), which was recently shown to be recruited to the ER membrane in a GABARAPL2-dependent manner (Huber et al., 2019). By subjecting lysates derived from parental and GABARAPL2^{endoHA} cells that were transiently transfected with Myc–UBA5 or left untreated to HA IPs, we confirmed the GABARAPL2–UBA5 interaction (Fig. 6A), and demonstrated that it occurs at endogenous expression levels (Fig. 6B). Since ACSL3 binds GABARAPL2 at the ER membrane, we investigated whether ACSL3 also colocalizes with UBA5. Indeed, immunolabeling of fixed GABARAPL2^{endoHA}/ACSL3^{endoNeonGreen} cells with an anti-UBA5 antibody followed by SRRF imaging showed partially colocalization of UBA5 and ACSL3 (Fig. 6C). Moreover, when we labeled GABARAPL2^{endoHA}/ACSL3^{endoNeonGreen} cells with anti-UBA5 and anti-HA antibodies, we also observed triple localization of ACSL3, GABARAPL2 and UBA5 (Fig. 6D). Next, we examined the effect of GABARAPL2 depletion on the ACSL3–UBA5 interaction. For this, we transfected HeLa cells stably overexpressing ACSL3–HA with Myc–UBA5 and a siRNA against GABARAPL2 or a non-targeting control followed by HA IP. Consistent with the notion that GABARAPL2 recruits UBA5 to ACSL3, we observed a clear reduction of UBA5 levels in ACSL3 immunoprecipitates upon GABARAPL2 knockdown (Fig. 6E). Finally, we asked whether the ACSL3–UBA5 interaction is modulated by lipid stress. To address this question, we performed Myc IPs on lysates derived from Myc–UBA5-transfected mock or

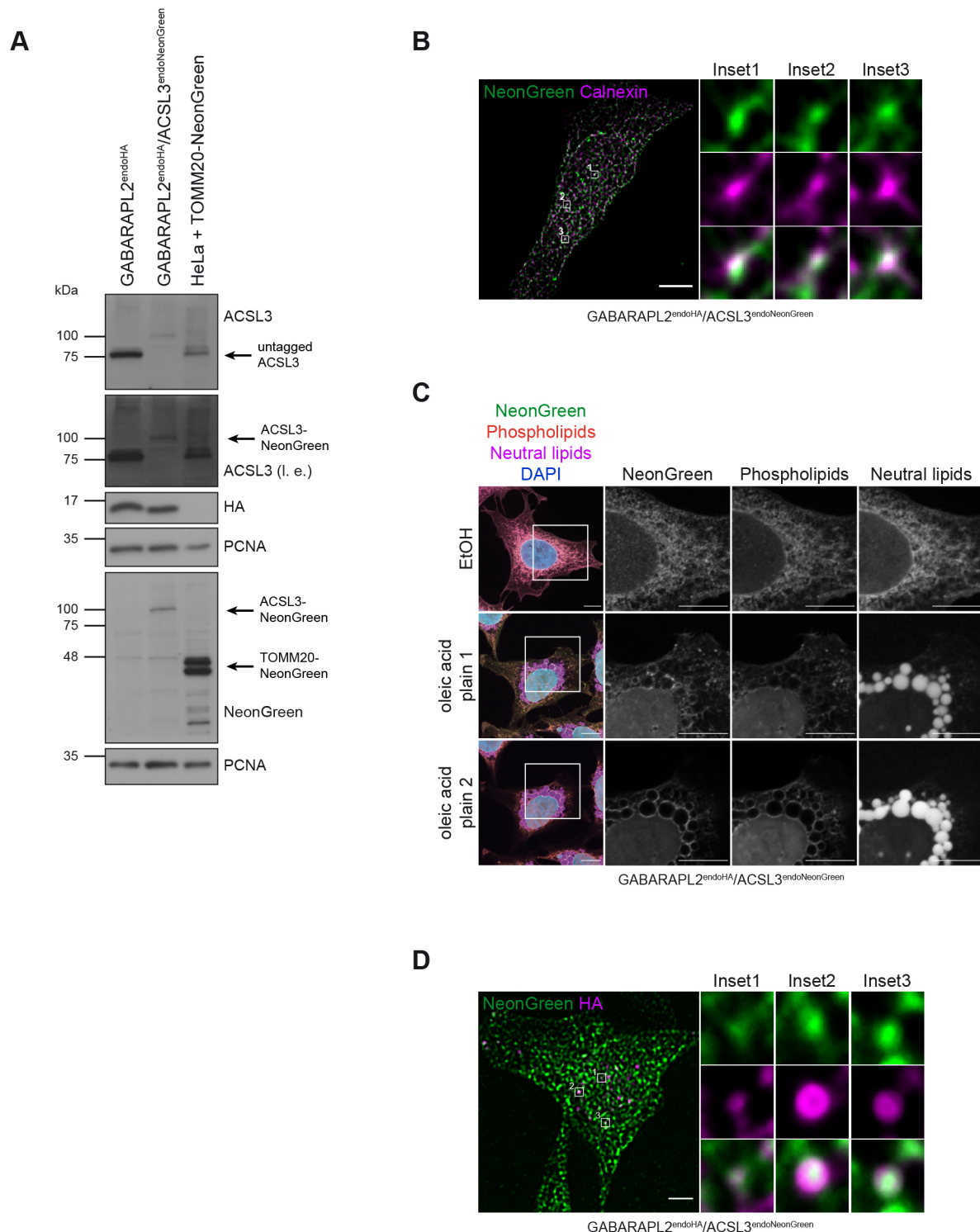


Fig. 4. Colocalization of GABARAPL2 and ACSL3 at the ER. (A) GABARAPL2^{endoHA} and GABARAPL2^{endoHA}/ACSL3^{endoNeonGreen} cells as well as parental HeLa cells transiently transfected with TOMM20–NeonGreen were lysed and analyzed by immunoblotting with indicated antibodies. I.e., long exposure. (B) Representative SRRF image of GABARAPL2^{endoHA}/ACSL3^{endoNeonGreen} cells immunolabeled with anti-calnexin. Magnified view of colocalization events of ACSL3^{endoNeonGreen} and the ER marker calnexin are also shown. (C) GABARAPL2^{endoHA}/ACSL3^{endoNeonGreen} cells were treated with oleic acid or ethanol (EtOH; control) for 24 h followed by fixation and labeling of phospholipids and neutral lipids with HCS LipidTox lipid stains. Two confocal planes are shown for oleic acid treatment. (D) Representative SRRF image of GABARAPL2^{endoHA}/ACSL3^{endoNeonGreen} cells after immunolabeling with anti-HA. Images labeled insets show magnified view of colocalization events. Scale bars: 5 μ m (B,D), 10 μ m (C).

ACSL3–HA-expressing HeLa cells that were grown in the absence and presence of oleic acid. Remarkably, we found that UBA5 associates with ACSL3 independently of its activity during LD

formation (Fig. 6F). Overall, these results suggest that ACSL3, GABARAPL2 and UBA5 form a complex at the ER membrane in a GABARAPL2-dependent manner.

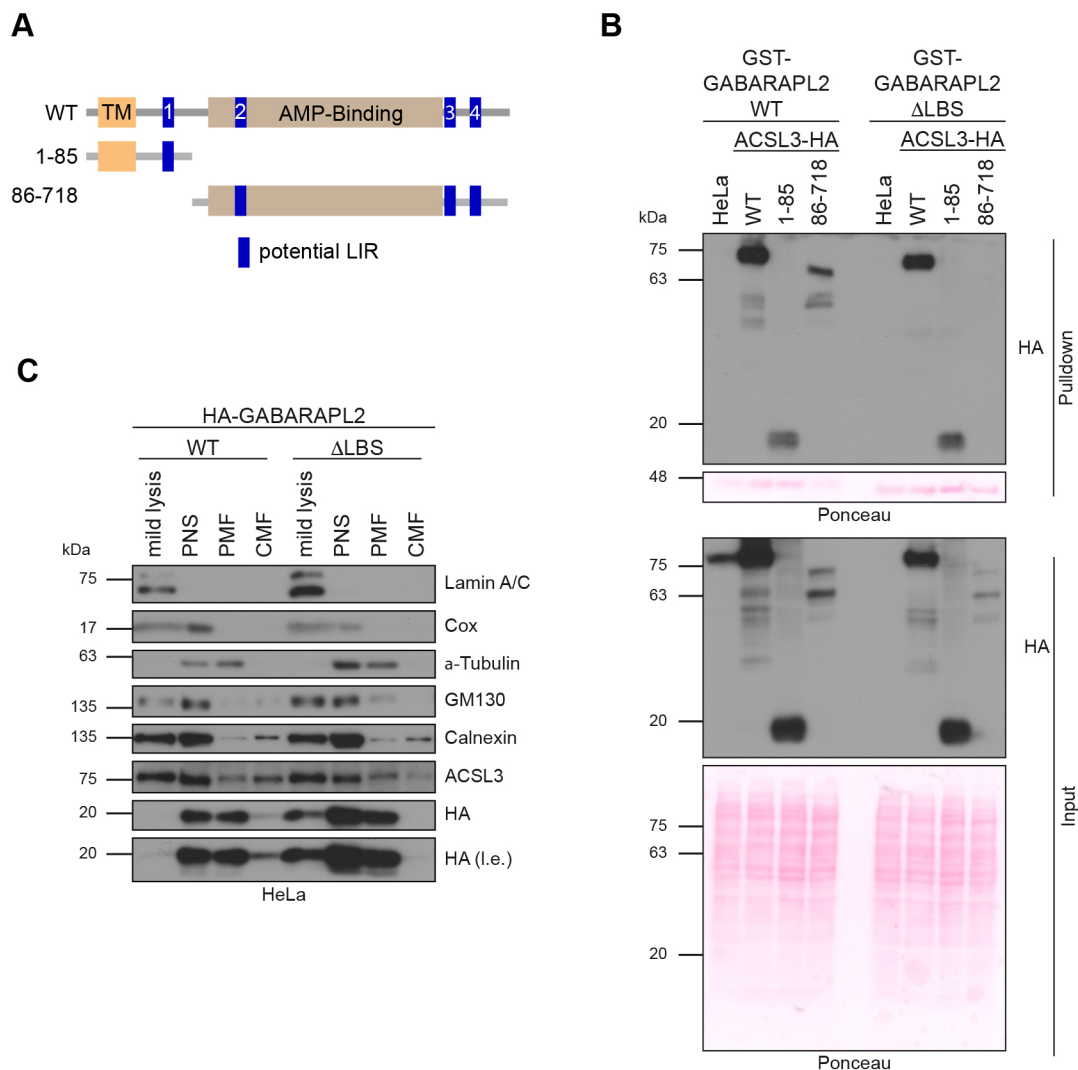


Fig. 5. LDS of GABARAPL2 mediate ACSL3 binding and ER recruitment. (A) Scheme of wild-type (WT) ACSL3 and fragments with known domains and potential LIRs. (B) Pulldown assays using GST-tagged WT or ΔLBS GABARAPL2 protein incubated with lysates from HeLa cells expressing WT or fragmented ACSL3 analyzed by immunoblotting and Ponceau staining. (C) Subcellular fractionation of HeLa cells stably expressing WT or ΔLBS GABARAPL2 followed by immunoblot analysis with indicated antibodies. PNS, post nuclear fraction; PMF, post mitochondrial fraction; CMF, crude microsomal fraction; l.e., long exposure.

ACSL3 regulates ufmylation pathway components

Since we found that ACSL3 stabilizes GABARAPL2, we investigated whether ACSL3 depletion has similar effects on UBA5 protein abundance. For this purpose, GABARAPL2^{endoHA} cells were transfected with siRNA against ACSL3 or a non-targeting control, and grown in the absence or presence of BafA1 or Btz. Indeed, we observed that protein levels of UBA5 decreased upon ACSL3 depletion but they were not restored by blockage of autophagosomal or proteasomal degradation (Fig. 7A,B). By contrast, depletion of GABARAPL2 had no effect on UBA5 protein levels (Fig. 3B). This supports the notion that UBA5 and GABARAPL2 form a functional unit that is regulated by ACSL3. UBA5 is part of the conjugation system, termed ufmylation, that covalently attaches the ubiquitin-like protein ubiquitin fold modifier 1 (UFM1) to target proteins through an E1–E2–E3 multienzyme cascade. The E1-like enzyme UBA5 activates UFM1 by forming a thioester bond between its active site and the exposed C-terminal glycine of UFM1 (Komatsu et al., 2004). The UFM1-conjugating enzyme 1 (UFC1) then transfers UFM1 from UBA5 to the UFM1-

protein ligase 1 (UFL1) which mediates the attachment to target proteins (Komatsu et al., 2004; Tatsumi et al., 2010). While UFC1 is cytosolic, the ER-membrane bound protein DDRGK1 anchors UFL1 to the ER membrane (Wu et al., 2010) and is reported to be one of the few known ufmylation targets besides RPL26 (Walczak et al., 2019), RPN1 (Liang et al., 2020) and ASC1 (Yoo et al., 2014; Tatsumi et al., 2010). While the consequences of ufmylation remains poorly understood at the mechanistic level, the UFM1 conjugation pathway has been linked to the ER stress response (Lemaire et al., 2011; Zhang et al., 2012), erythrocyte differentiation (Cai et al., 2015; Tatsumi et al., 2011), cellular homeostasis (Zhang et al., 2015) and breast cancer progression (Yoo et al., 2014). Since the stability of UBA5 and its ER-recruiting factor GABARAPL2 was controlled by ACSL3, we probed whether it also regulates the abundance of the other proteins in the ufmylation cascade. Knockdown experiments revealed that the protein levels of UFL1 and DDRGK1 were significantly decreased upon ACSL3 depletion, while the abundance of UFC1 was significantly increased. Conjugated UFM1 levels were largely unchanged

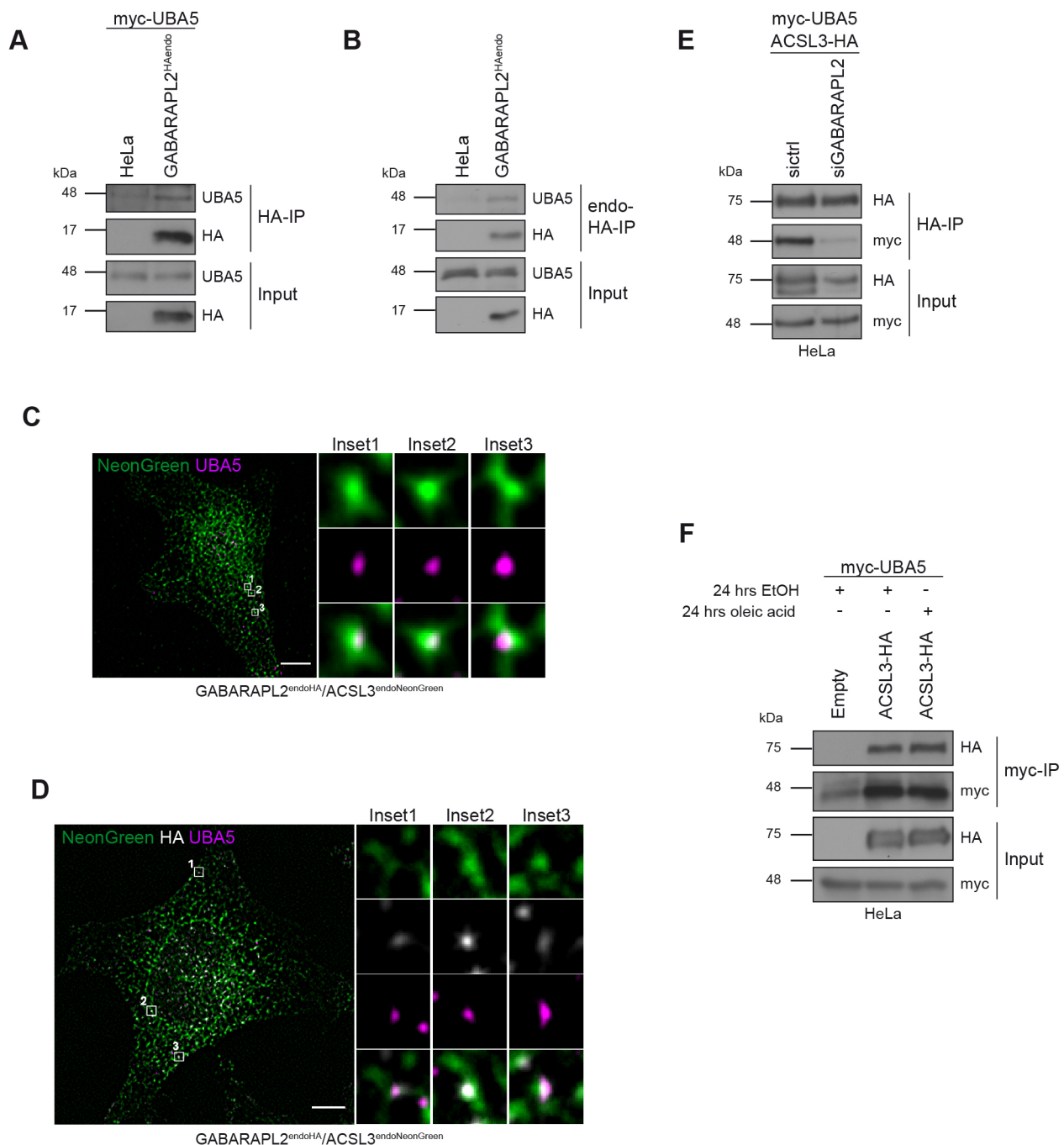


Fig. 6. UBA5 binds to and colocalizes with ACSL3 and GABARAPL2. (A,B) Immunoblot analysis of anti-HA immunoprecipitates from lysates derived from parental HeLa and GABARAPL2^{endoHA} cells either transiently transfected for 48 h with Myc-UBA5 (A) or left untreated (B) and analyzed with indicated antibodies. (C) Representative SRRF image of GABARAPL2^{endoHA}/ACSL3^{endoNeonGreen} cells immunolabeled with anti-UBA5. Colocalization events of ACSL3^{endoNeonGreen} and UBA5 are shown enlarged in insets. (D) Representative SRRF image of GABARAPL2^{endoHA}/ACSL3^{endoNeonGreen} cells labeled with anti-HA and -UBA5. Colocalization events of ACSL3^{endoNeonGreen}, GABARAPL2^{endoHA} and UBA5 are shown in magnified images. (E) Stably expressing ACSL3-HA cells were reverse transfected with siGABARAPL2 for 72 h and transiently transfected with Myc-UBA5 for 48 h followed by lysis, anti-HA immunoprecipitation and immunoblot analysis. (F) Parental HeLa and GABARAPL2^{endoHA} cells transfected with Myc-UBA5 were treated with oleic acid or ethanol (EtOH) for 24 h prior to lysis, anti-Myc immunoprecipitation and immunoblotting. Scale bars: 5 μ m.

(Fig. 7A,B; Fig. S4C). The observation that the protein levels of UBA5, UFL1 and DDRGK1 were not restored by blockage of autophagy or the proteasome (Fig. 7A,B) indicates that these ufmylation factors are most likely regulated at the transcriptional level. Together, this suggests that ACSL3 not only anchors UBA5 but might act as novel regulator of the ufmylation cascade.

LDs regulate UFM1 conjugation and ER-phagy

The finding that the LD biogenesis factor ACSL3 stabilizes several components of the UFM1 conjugation pathway raises the question of whether LD biogenesis and ufmylation are functionally coupled. To test this hypothesis, we monitored the ufmylation pathway in response to induction of LD formation in GABARAPL2^{endoHA} cells

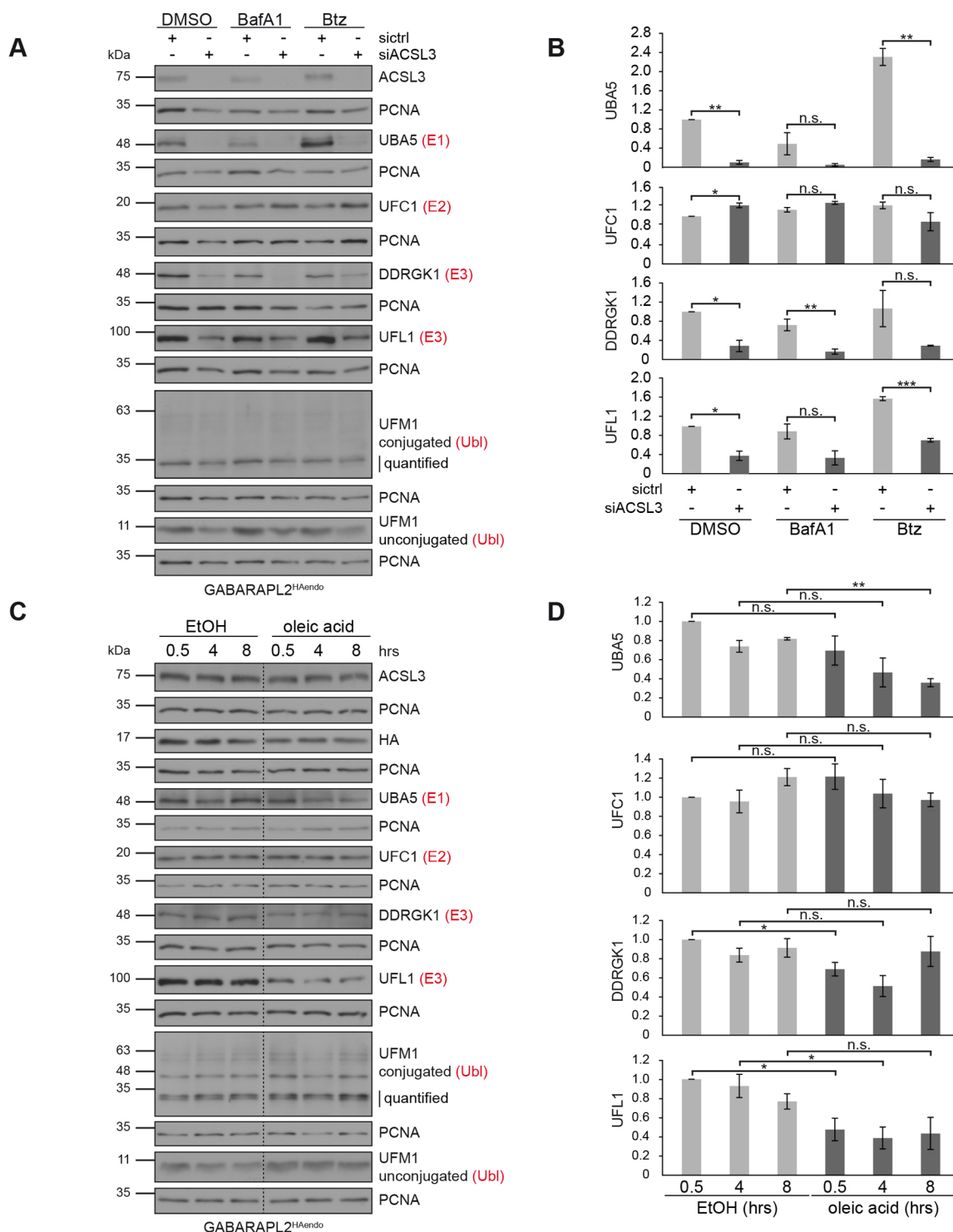


Fig. 7. ACSL3 and LD biogenesis regulate the ufmylation pathway. (A) GABARAPL2^{endoHA} cells were transfected with ACSL3 siRNAs and treated with Btz or BafA1 followed by lysis and immunoblot analysis using indicated antibodies. (B) Quantitative analysis of A. Data represents mean±s.e.m. Statistical analysis ($n=3$) of the indicated protein:PCNA ratio normalized to siCtrl-DMSO was performed using Student's *t*-test (* $P<0.05$, ** $P<0.01$, *** $P<0.001$). (C) GABARAPL2^{endoHA} cells were treated with oleic acid or EtOH for 0.5, 4 or 8 h prior to lysis and immunoblotting with indicated antibodies. (D) Quantitative analysis of C. Data represents mean±s.e.m. Statistical analysis ($n=3$) of the indicated protein:PCNA ratio normalized to 0.5 h ethanol (EtOH) was performed using Student's *t*-test (* $P<0.05$, ** $P<0.01$). n.s., not significant.

grown in the absence and presence of oleic acid for 0.5, 4 and 8 h, respectively. While UBA5 levels significantly decreased in the course of 8 h oleic acid treatment, there was no effect on UFC1 (Fig. 7C,D). In contrast, the protein levels of DDRGK1 and UFL1

both decreased in the first 4 h of incubation with oleic acid but, after 8 h, at least DDRGK1 levels, were almost restored (Fig. 7C,D). Interestingly, we detected significantly more conjugated UFM1 (~35 kDa) after 4 h of oleic acid incubation (Fig. S4D), which

might be due to altered ufmylation and de-ufmylation dynamics. Given that LD formation induced a substantial suppression of several ufmylation components and that these components were recently shown to be required for starvation-induced ER sheet-targeting selective autophagy (Liang et al., 2020), we examined whether induction of LD blocks this ER-phagy pathway. To this end, we employed the recently developed ER-autophagy tandem reporter system, which allows the quantification of reticulolysosomes (Liang et al., 2018). Briefly, HeLa cells were

transfected with mCherry–eGFP–RAMP4 and starved by culture in Earle's balanced salt solution (EBSS) for 8 h in combination with either ethanol or oleic acid. As expected, we observed a robust decrease in the numbers of red-only puncta, which indicates reduced numbers of reticulolysosomes and hence an inhibition of ER-phagy following LD formation (Fig. 8A,B). Together, these results indicate that the ufmylation cascade is differentially regulated during induction of LDs, and that the ACSL3–GABARAPL2–UBA5 axis plays an important part in this regulation.

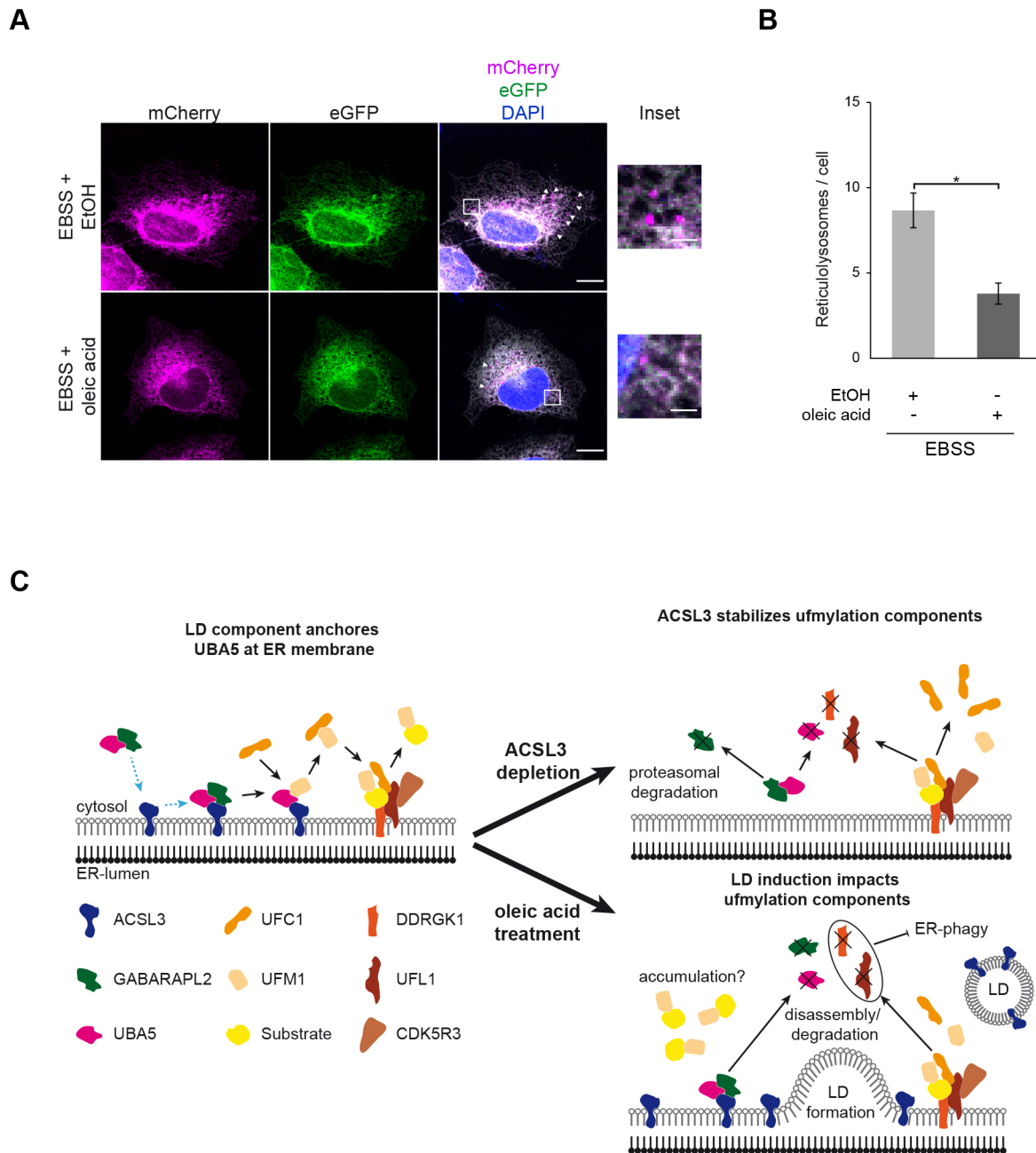


Fig. 8. Oleic acid inhibits ER-phagy. (A) HeLa cells were transiently transfected with mCherry–eGFP–RAMP4 and starved with EBSS for 8 h in combination with either ethanol (EtOH) or oleic acid. Red-only puncta were defined as reticulolysosomes. Scale bars: 10 μ m (main image); 2 μ m (inset image). Arrowheads indicate reticulolysosomes. (B) Quantitative analysis of A. Data represents mean \pm s.e.m. Statistical analysis ($n=3$) was performed using Student's t -test ($*P<0.05$). (C) Working model of the role of ACSL3 in the ufmylation pathway. UBA5 is recruited to ACSL3 by GABARAPL2. Upon loss of ACSL3 or induction of LD biogenesis, ufmylation components are downregulated and dynamics of UFM1 conjugation are altered. Dotted blue arrows indicate ER recruitment, black arrows indicate the ufmylation cascade.

DISCUSSION

In this study, we identified the ER-associated LD biogenesis factor ACSL3 as novel binding partner of GABARAPL2 and the UFM1-activating enzyme UBA5 using a CRISPR/Cas9-generated GABARAPL2^{endoHA} cell line. Furthermore, we provide evidence for a role of ACSL3 and LD biogenesis in the regulation of ufmylation.

In our interactome screen with endogenously tagged GABARAPL2, we found ACSL3, which we confirmed as a GABARAPL2 interactor by immunoprecipitations, GST pulldowns and SRRF imaging. Moreover, our data suggest that this interaction is mediated by a LIR and one additional binding motif in ACSL3. By using GABARAPL2 LIR-binding deficient mutants, as well as N- and C-terminal ACSL3 fragments, we narrowed down the LIR in ACSL3 as being within amino acids 86–718, thereby excluding candidate LIR-1. Given that candidate LIR-2 is localized within the AMP-binding domain of ACSL3 and therefore unlikely accessible, candidate LIR-3 or -4 might mediate the binding to the LDS of GABARAPL2 (Fig. S4A). In addition, our binding studies indicate that there is a GABARAPL2 LDS-independent binding motif within residues 1–85 of ACSL3. In addition to the LIR/LDS pairing, Marshall and colleagues recently reported an alternative hATG8 interaction modus in which binding partners employ a ubiquitin-interacting motif (UIM) to bind to an UIM-docking site (UDS) in LC3 and GABARAP proteins (Marshall et al., 2015). According to the UIM consensus sequence (Marshall and Vierstra, 2019), we indeed found a potential UIM (amino acids 73–81) in ACSL3 by manual sequence inspection (Fig. S4A). However, this candidate UIM is reversed in its sequence, similar to what is seen with inverted SUMO interaction motifs (Matic et al., 2010). Whether and how this UIM binds to the UDS of GABARAPL2 remains to be structurally determined. Importantly, our subcellular fractionation assay revealed that GABARAPL2 recruitment to the ER membrane is dependent on the LIR of ACSL3 as the LDS GABARAPL2 mutant was dramatically reduced in the ER membrane fractions compared to wild-type GABARAPL2.

GABARAP proteins were shown to mediate ER recruitment of UBA5 to bring it in close proximity to the membrane-bound UFM1 E3 enzyme complex composed of UFL1, DDRGK1 and CDK5R3, thereby facilitating ufmylation (Huber et al., 2019). However, since GABARAPs are not known to be conjugated to PE at the ER, the molecular basis of this recruitment process was not clear. Here, we provided evidence that the function of ACSL3 was to anchor UBA5 at the ER membrane. Given that UBA5 employs an atypical LIR to bind both GABARAPL2 and UFM1, and that the latter is able to outcompete GABARAPL2 binding of UBA5 *in vitro* (Habisov et al., 2016), it is tempting to speculate that GABARAPL2 interacts with UBA5 until UFM1 conjugation is triggered. In this scenario, GABARAPL2 is a recruiting factor that hands UBA5 over to ACSL3 (Fig. 8C). However, the binding mode of ACSL3 and UBA5 remains to be explored.

While targets of ufmylation are still largely unknown, three of the known UFM1-modified proteins are linked to the ER. Firstly, UFM1 conjugation of DDRGK1 is essential for the stabilization of the serine/threonine-protein kinase/endoribonuclease inositol-requiring enzyme 1 (IRE1; also known as ERN1) (Liu et al., 2017; Yoo et al., 2014). Secondly, it was shown that the 60S ribosomal protein L26 (RPL26) is exclusively ufmylated and de-ufmylated at the ER membrane (Walczak et al., 2019). Thirdly, ribophorin 1 (RPN1), an ER transmembrane protein and part of the oligosaccharyltransferase complex, is ufmylated in a DDRGK1-dependent manner (Liang et al., 2020; Kelleher et al., 1992). Overall, emerging evidence points to a role of the UFM1 conjugation system as regulator of ER homeostasis, the ER stress

response and ER remodeling. Disruption of protein folding and accumulation of unfolded proteins in the ER are hallmarks of ER stress, which leads to the induction of the unfolded protein response (UPR) via one of these three key factors: IRE1, PKR-like ER protein kinase (PERK) or activating transcription factor 6 (ATF6). Protein degradation, reduction of protein synthesis and enlargement of the ER capacity are part of the UPR (Karagöz et al., 2019). In different cell lines and animal models, it was reported that ufmylation is upregulated via IRE1 or PERK upon ER stress, while depletion of ufmylation components induce the UPR (Gerakis et al., 2019; Lemaire et al., 2011; Zhang et al., 2015, 2012; Zhu et al., 2019). Upon re-established ER homeostasis, ufmylation coordinates the elimination of extended ER membranes through ER-phagy (Liang et al., 2020; DeJesus et al., 2016).

In our present study, we identified LD formation stimulated by oleic acid treatment as a novel regulator of ufmylation. LD biogenesis starts with lens formation, an accumulation of neutral lipids between the ER membrane leaflets until LDs eventually bud from the ER. The hydrophobic neutral lipid core of a LD is surrounded by a phospholipid monolayer with the origin of the outer ER membrane leaflet (Henne et al., 2018). ACSL3 was identified as an LD-associated protein and being essential for LD biogenesis, expansion and maturation (Fujimoto et al., 2004; Kassan et al., 2013). During initiation of LD biogenesis ACSL3 is translocated and concentrated to pre-LDs to drive LD expansion by mediating acyl-CoA synthesis. However, cells with enzymatically inactive ACSL3 are still able to form LDs, suggesting additional functions of ACSL3 in LD biogenesis (Kassan et al., 2013; Kimura et al., 2018). Induction of LD formation induced by oleic acid, which requires ACSL3, resulted in a reduction of UBA5, UFL1 and DDRGK1 protein levels and thus potentially shut down of UFM1 conjugation (Figs 7C,D and 8C). Interestingly, depletion of ACSL3 led to a similar phenotype with regard to these three ufmylation components. Together, these results suggest that ACSL3 regulates UBA5, DDRGK1 and UFL1 protein levels, and therefore ufmylation (Fig. 8C). The observation that inhibition of proteasomal or lysosomal degradation did not rescue this phenotype suggests that these components of the ufmylation machinery are probably downregulated at the transcriptional level. To what extent this involves one of the three UPR factors IRE1, PERK or ATF6 remains to be examined. Consistent with the recent finding that ER-phagy is blocked by inhibition of the interaction between DDRGK1 and UFL1 (Liang et al., 2020), we observed that LD biogenesis inhibits the remodeling of ER membranes by ER-phagy. While DDRGK1 protein levels are restored 8 h after induction of LD formation, it needs to be further investigated when UFL1 protein levels are reestablished and therefore ER-phagy is restored.

Collectively, these findings underline the potential of our CRISPR/Cas9 gene-edited cell lines to uncover novel cellular pathways involving hATG8 family members without the need of overexpression systems, thereby complementing the recently generated LC3- and GABARAP-knockout cell lines (Nguyen et al., 2016). Together with the LC3C^{endoHA} cell line that we previously reported (Le Guerroué et al., 2017), this cellular resource circumvents the drawback of unspecific LC3 and GABARAP antibodies, and hence will greatly facilitate the functional dissection of individual hATG8 proteins.

MATERIALS AND METHODS

Cell culture and treatments

HeLa cell lines were cultured in Dulbecco's modified Eagle's medium (DMEM) plus GlutaMAX-I (Gibco) supplemented with 10% fetal bovine

serum (FBS) and 1 mM sodium pyruvate (Gibco) and grown at 37°C and 5% CO₂. For SILAC mass spectrometry, cells were grown in lysine- and arginine-free DMEM (Gibco) supplemented with 10% dialyzed FBS, 2 mM glutamine (Gibco), 1 mM sodium pyruvate (Gibco) and 146 mg/ml light (K0, Sigma) or heavy L-lysine (K8, Cambridge Isotope Laboratories) and 84 mg/ml light (R0, Sigma) or heavy L-arginine (R10, Cambridge Isotope Laboratories). SILAC-labeled cells were counted after harvesting, mixed 1:1 and stored at −80°C. For selection, puromycin (2 µg/ml) or blasticidine (4 µg/ml) was added to the growth medium. The following reagents were used for treatments: oleic acid (EMD Millipore, 4954, 600 µM in ethanol for 0.5, 4, 8 or 24 h), Bafilomycin A1 (Biomol, Cay11038-1, 200 nM in DMSO for 2 h), Torin1 (Tocris, 4247, 250 nM in DMSO for 2 h), Bortezomib (LC Labs B-1408, 1 µM in PBS for 8 h), ATG7 inhibitor (Takeda ML00792183, 1 µM in DMSO for 24 h), EBSS (Sigma E2888, for 8 h) and doxycycline hyclate (Sigma D9891, 4 µg/ml for 24 h).

Plasmids and stable cell lines

attB-flanked open reading frames (ORFs), generated by PCR were cloned into the Gateway entry vector pDONR233. ORFs from pDONR233 constructs were introduced into one of the following destination vectors using recombination cloning: pHAGE-N-Flag-HA, pHAGE-C-FLAG-HA (Dana Farber/Harvard Cancer Center DNA Resource Core), pET-60-DEST (Merck Millipore), pEZYmyc-HIS (Addgene #18701) or pDEST-myc (Thermo Fisher Scientific). Stable HA-GABARAPL2- and ACSL3-HA-expressing cells were generated by lentiviral transduction followed by selection with 2 µg/ml puromycin. pEZY and pDEST constructs were used for transient expression in cells (see Transfection section below).

Site-directed mutagenesis

For site-directed mutagenesis, primers were designed with QuikChange Primer Design software (Agilent Technologies). First, forward and reverse primers were used in individual PCRs using KOD Hot Start polymerase (Merck Millipore), according to the instruction of the manufacturer, with the appropriate pDONOR-ORF plasmid as template. In a second step, PCRs were combined and plasmids with the mutated ORF were generated through a second round of PCR. The obtained PCR mixture was purified with QIAquick PCR purification kit (Qiagen, 28104) and mutated plasmids were amplified in *E. coli*. Mutagenesis was verified by sequencing the purified plasmid.

Genome editing

The N-terminal HA-tagged hATG8 cell lines were generated with homology PCR templates containing 87 bp of the GABARAP, GABARAPL1, GABARAPL2 or LC3B 5'UTR including the start codon followed by the blasticidine resistance gene, P2A, HA and 92 bp downstream of the start codon of the corresponding hATG8 gene. For the C-terminal ACSL3-NeonGreen cell line, we used a homology PCR template containing 75 bp of the last exon of ACSL3, the NeonGreen ORF (Allele Biotech), T2A and the blasticidine resistance gene ending with 84 bp downstream of the last exon of ACSL3. sgRNAs for hATG8s and ACSL3, designed with the online design tool from the Broad Institute (<https://portals.broadinstitute.org/gpp/public/analysis-tools/sgRNA-design>) were cloned into BspI digested px330 (Addgene #42230), a SpCas9-expressing plasmid (sgRNA: GABARAP, 5'-GGAGGATGAAGTTCGTGTAC-3'; GABARAPL1, 5'-TGCGGTGCA-TCATGAAGTTC-3'; GABARAPL2, 5'-CCATGAAGTGGATGTTCAA-G-3'; LC3B, 5'-AGATCCCTGCACCATGCCGT-3'; ACSL3, 5'-AGAAAATAATTATTCTTCTC-3'). HeLa cells were seeded in a six-well plate and transfected, using Lipofectamine 2000 according to the manufacturer's instructions, with sgRNA and the corresponding homology PCR template. After 48 h, cells were selected with 4 µg/ml blasticidine and subjected to single-cell selection in 96-well plates. Cells with mNeonGreen insertion were sorted by FACS. Correct introduction of the tag was verified by PCR and sequencing.

Antibodies and dyes

For immunoblotting the following primary antibodies were used at a concentration of 1:1000 in 5% milk in 20 mM Tris-HCl pH 7.4, 150 mM NaCl and 0.1% Tween-20 (TBS-T) or 5% BSA-TBS-T or 0.2% I-Block-

TBS-T [ACSL3 (Santa Cruz Biotechnology, sc-166374), α -tubulin (Abcam, ab64503), ATG7 (Cell Signaling, 8558), Calnexin (Cell Signaling, 2433), c-Myc (Bethyl, A190-104A), COXIV (Cell Signaling, 4850), DDRGK1 (Sigma, HPA013373), GM130 (Abcam, ab52649), HA (Cell Signaling, 3724S/Biolegend, 901501), LaminA/C (Abcam, ab108595), mNeonGreen (Chromotek, 32F6), PCNA (Santa Cruz Biotechnology, sc-7907), p62 (MBL, PM045/BD, 610832), UBA5 (Proteintech, 12093-1-AP/Sigma, HPA017235), UFC1 (Proteintech, 15783-1-AP), UFL1 (Abcam, ab226216), UFM1 (Abcam, ab109305)] or at a concentration of 1:100 in 5% milk-TBS-T [c-Myc (Monoclonal Antibody Core Facility, Helmholtz Zentrum Munich, 9E1, rat IgG1), c-Myc (Monoclonal Antibody Core Facility, Helmholtz Zentrum Munich, 9E10, mouse IgG)]. As secondary antibodies, we used horseradish peroxidase coupled anti-mouse-IgG (Promega, W402B), anti-rabbit-IgG (Promega, W401B) and anti-goat-IgG (Dianova, 705035003) antibodies at a concentration of 1:10,000 and anti-rat IgG1 (Monoclonal Antibody Core Facility, Helmholtz Zentrum Munich) antibody at a concentration of 1:100 in 1% milk-TBS-T or 1% BSA-TBS-T or 0.2% iBlock-TBS-T. The following primary antibodies and lipid stains were used for immunofluorescence in 0.1% BSA-PBS: calnexin (Stressgen, SPA-860, 1:100), HA (Roche, 11867423001, 1:50), LAMP1 (DSHB, H4A3, 1:50), LC3 (MBL, PM036, 1:500), p62 (BD, 610832, 1:500), SEC13 (Novus, AF9055-100, 1:300), HCS LipidTOX™ Red Phospholipidosis Detection Reagent (Thermo Scientific, H34351, 1:1000) and HCS LipidTOX™ Deep Red Neutral Lipid Stain (Thermo Scientific, H34477, 1:500). The following fluorophore-conjugated secondary antibodies from Thermo Fisher were used at a concentration of 1:1000 in 0.1% BSA-PBS: anti-mouse-IgG Alexa Fluor 488 (A-11001), anti-rabbit-IgG Alexa Fluor 488 (A-11008) and anti-rat-IgG Alexa Fluor 647 (A-21247).

Transfection

For siRNA knockdowns, cells were reversely transfected with Lipofectamine RNAiMax (Thermo Fisher Scientific) according to the manufacturer's guidance with 30 nM of the following siRNAs from Dharmacon/Horizon Discovery and harvested 72 h after transfection: siCtrl, 5'-UGGUUUACAUGUUUUUCCUA-3'; siACSL3#1, 5'-UAACUGAAC-UAGCUCGAAA-3'; siACSL3#2, 5'-GCAGUAAUCAUGUACACAA-3'; siGABARAP, 5'-GGUCAGUUCUACUUCUUGA-3'; siGABARAPL1, 5'-GGACCAUCCCUUGAGUAU-3'; siGABARAPL2, 5'-GCUCAGU-UCAUGUGGAUCA-3'; and siLC3B, 5'-GUAGAAGAUGUCCGACUU-A-3'. Plasmids were transiently transfected with Lipofectamine 2000 (Thermo Fisher Scientific) according to the instruction of the manufacturer or with 10 mM PEI (Polyethylenimine) and cells were collected after 48 h.

Immunoblotting

Cells were lysed in RIPA buffer [50 mM Tris-HCl pH 7.4, 150 mM NaCl, 0.5% sodium desoxycholate, 1% NP-40, 0.1% SDS, 1× EDTA-free protease inhibitor (Roche) and 1× phosphatase inhibitor (Roche)] for 30 min. After elimination of cell debris by centrifugation (20,000 *g* for 10 min), proteins were diluted with 3× loading buffer (200 mM Tris-HCl pH 6.8, 6% SDS, 20% glycerol, 0.1 g/ml DTT and 0.1 mg Bromophenol Blue) and boiled at 95°C. Proteins were size separated by SDS-PAGE with self-casted 8%, 10%, 12% and 15% gels followed by protein transfer onto nitrocellulose membranes (GE Healthcare Life Sciences, 0.45 µm). For better visibility of endogenous HA-hATG8s, membranes were boiled for 5 min in PBS after protein transfer. For GST pulldowns, equal sample loading was confirmed with 5 min Ponceau staining (0.2% Ponceau S, 3% acetic acid) followed by a 10 min TBS-T washing step. Blots were blocked in TBS-T supplemented with 5% low-fat milk (Roth) or 5% BSA (Sigma) or 0.2% I-Block protein-based blocking reagent (Thermo Fisher) for 1 h. Primary antibodies were incubated with membranes overnight followed by several wash steps with TBS-T and incubation with secondary antibodies for 1 h at room temperature. After repeated washing, immunoblots were analyzed with Western Lighting Plus ECL (Perkin Elmer).

Immunofluorescence

All steps were carried out at room temperature. Cells growing on glass coverslips in 12-well plates were fixed with 4% paraformaldehyde in PBS

for 15 min followed by permeabilization with 0.1% Triton X-100 in PBS or 0.1% saponin in PBS for 15 min and 1 h blocking in 1% BSA-PBS. Primary and secondary antibody incubation was performed sequentially for 1 h at room temperature in 0.1% BSA-PBS followed by mounting of the coverslips with ProlongGold Antifade with Dapi (Thermo Fisher). In between each step, cells were washed several times with PBS. Cells were imaged with a LSM 800 Carl Zeiss microscope using 63× oil-immersion objective and ZEN blue edition software and analyses with ImageJ (version 1.52).

Sample preparation for SRRF imaging

For super-resolution radial fluctuations (SRRF; Culley et al., 2018) imaging, GABARAPL2^{endoHA}/ACSL3^{endoNeonGreen} cells were seeded on 18-mm-diameter coverslips at a density of 2×10^5 per 35 mm dish. Following overnight incubation, cells were fixed with 4% PFA for 15 min at room temperature, washed three times with 1× PBS followed by a 5 min additional washing with 50 mM NH₄Cl. Permeabilization was performed for 5 min with 0.5% Triton X-100 and blocking for 40 min in 1% BSA. The following antibodies were used at room temperature in 1% BSA for 1 h: rabbit polyclonal anti-Calnexin (Abcam, ab22595, 1:500), mouse monoclonal anti-HA (Sigma, H9658, 1:500) and rabbit polyclonal anti-UBA5 (PTGLab, 12093-a-AP, 1:250).

Acquisition of SRRF images

Confocal microscopy imaging of immunostained HeLa cells was performed on Andor Dragonfly spinning disk using a Nikon Ti2 inverted optical microscope [60× TIRF objective (Plan-APOCHROMAT 60×/1.49 oil)]. Fluorescence was collected with an EMCCD camera (iXon Ultra 888, Andor). Images were acquired using SRRF-Stream mode in Fusion (version 2.1, Andor) with additional 1.5× magnification. The following imaging parameters were used: SRRF frame count, 150; SRRF radially magnification, 4×; SRRF ring radius, 1.4 px, SRRF temporal analysis, mean and SRRF FPN correction; 75 frames.

Immunoprecipitation

Frozen cell pellets from 4×15 cm cell culture plates for mass spectrometry or 2×10 cm cell culture plates for immunoblotting were lysed in glycerol buffer (20 mM Tris-HCl pH 7.4, 150 mM NaCl, 5 mM EDTA, 0.5% Triton-X-100, 10% glycerol, 1× protease inhibitor, 1× phosphatase inhibitor) for 30 min at 4°C with end-over-end rotation. Lysates were cleared from cell debris by centrifugation (20,000 g for 10 min) prior to adjustment of protein concentrations between the samples and overnight immunoprecipitation at 4°C with pre-equilibrated anti-HA-agarose (Sigma) or anti-c-Myc-agarose (Thermo Fisher). Agarose beads were washed five times with glycerol buffer followed by elution of proteins with 3× loading buffer and boiling of the samples at 95°C. Samples were then analyzed by SDS-PAGE (self-casted or BioRad 4–20% gels) followed by immunoblotting or in-gel tryptic digestion.

Mass spectrometry

SDS-PAGE gel lines were cut in 12 equal size bands, further chopped in smaller pieces and placed in 96-well plates (one band per well). Gel pieces were washed with 50 mM ammonium bicarbonate (ABC)/50% ethanol buffer followed by dehydration with ethanol, reduction of proteins with 10 mM DTT in 50 mM ABC at 56°C for 1 h and alkylation of proteins with 55 mM iodoacetamide in 50 mM ABC at room temperature for 45 min. Prior to overnight trypsin digestion (12 ng/μl trypsin in 50 mM ABC, Promega) at 37°C, gel pieces were washed and dehydrated as above. Peptides were extracted from gel pieces with 30% acetonitrile/3% trifluoroacetic acid (TFA), 70% acetonitrile and finally 100% acetonitrile followed by desalting on custom-made C18-stage tips. Using an Easy-nLC1200 liquid chromatography (Thermo Scientific), peptides were loaded onto 75 μm×15 cm fused silica capillaries (New Objective) packed with C18AQ resin (Reprosil-Pur 120, 1.9 μm, Dr. Maisch HPLC). Peptide mixtures were separated using a gradient of 5–33% acetonitrile in 0.1% acetic acid over 75 min and detected on a Q Exactive HF mass spectrometer (Thermo Scientific). Dynamic exclusion was enabled for

30 s and singly charged species or species for which a charge could not be assigned were rejected. MS data were processed with MaxQuant (version 1.6.0.1) and analyzed with Perseus (version 1.5.8.4, <http://www.coxdocs.org/doku.php?id=perseus:start>). IP experiments from GABARAPL2^{endoHA} and control parental HeLa cells were performed in duplicates and triplicates, respectively. Matches to common contaminants, reverse identifications and identifications based only on site-specific modifications were removed prior to further analysis. Log2 heavy:light ratios were calculated. A threshold based on a log2 fold change of greater than 1.5-fold or less than −1.5-fold was chosen so as to focus the data analysis on a smaller set of proteins with the largest alterations in abundance. Additional requirements were at least two MS counts, unique peptides and razor peptides, as well as absence in IPs from parental HeLa control cells. For functional annotations, the platform DAVID (<https://david.ncifcrf.gov/>) was used.

Subcellular fractionation

For isolation of the endoplasmic reticulum the endoplasmic reticulum isolation kit (Sigma, ER0100), was used and all steps were carried out according to the manufacturer's guidance. Each sample consisted of cells derived from 4×10 cm cell culture plates.

Protein expression and purification

For protein expression and purification, pET-60-DEST plasmids containing wild-type or mutant versions of GABARAPL2 were transformed in Rosetta *E. coli*. Bacteria were grown in LB medium at 37°C at 200 rpm and induced with 1 mM IPTG when an optical density at 600 nm (OD₆₀₀) of 0.5–0.6 was reached. After 4 h, bacteria were harvested by centrifugation (5000 g for 15 min) and resuspended in lysis buffer (150 mM NaCl, 50 mM Tris-HCl pH 8.0, 100 μg/ml Lysozyme, 1 mM PMSF and 1 mM DTT) and sonified at an amplitude of 50% for 10 min (30 s sonification/30 s break). Lysates were cleared from cell debris by centrifugation (30,000 g for 30 min) and incubated overnight with pre-equilibrated glutathione–Sephacrose 4B (GE Healthcare) at 4°C with end over end rotation. Glutathione beads were washed with 150 mM NaCl, 50 mM Tris-HCl pH 8.0, and GST-tagged proteins were eluted with 10 mM reduced glutathione in 50 mM Tris-HCl pH 8.0. GST-tagged proteins were dialyzed overnight in TBS with Slide-A-Lyzer cassettes (Thermo Fisher). Purified GST-tagged proteins were stored at −80°C until further usage.

Pulldown assay

Glutathione–Sephacrose 4B beads were always freshly coupled prior to the pulldown assay. For one reaction, 40 μl pre-equilibrated glutathione bead slurry was coupled to an appropriate amount of GST-tagged protein overnight at 4°C with end over end rotation. On the next day protein-coupled glutathione beads were washed with 150 mM NaCl, 50 mM Tris-HCl pH 8.0. Cells from 2×10 cm cell culture plates per sample were lysed in 600 μl glycerol buffer for 1 h. After clearance of cell debris by centrifugation (20,000 g for 10 min), lysates were precleared for 1 h at 4°C with pre-equilibrated uncoupled glutathione beads prior to the adjustment of protein concentrations. To ensure equal addition of the different GST-tagged proteins, protein–bead binding was monitored by serial dilutions on Coomassie-stained (0.1% Coomassie Brilliant Blue R, 40% ethanol, 10% acetic acid) acrylamide gels. Accordingly, coupled beads were diluted, and 40 μl per sample was added. After overnight incubation at 4°C, beads were washed with glycerol buffer and boiled for 5 min at 95°C.

ER-phagy assay

HeLa cells were seeded on glass coverslips in 12-well plates. The next day, cells were transfected with TETOn-mCherry-GFP-RAMP4 (Addgene plasmid #109014 deposited by Jacob Corn) at 500 ng per well with FuGENE[®] HD transfection reagent (Promega), using manufacturer's recommendations and in the presence of 4 μg/ml doxycycline. After 24 h, cells were placed into fresh complete DMEM, and doxycycline was removed. At 40 h after initial transfection, cells were starved with EBSS medium for 8 h in the presence of either ethanol or oleic acid. Cells were then fixed with 4% paraformaldehyde in PBS, pH 7.2 at room temperature for 10 min, washed 3×5 min with PBS, stained with 1:5000 DAPI in the

penultimate wash and mounted in Dako fluorescent mounting medium (Dako) onto glass slides. Images were captured with a Nikon A1R TiE confocal microscope using a 100×1.4 NA objective (Nikon Instruments). All confocal images are shown as z-projections of at least three z-steps. All quantifications were performed on a minimum of 90 cells across three biological replicates and the s.e.m. was determined for each data set. Cells were single blind scored for red-only puncta (autolysosomes).

Statistical analysis

Quantification and statistical analysis were undertaken with ImageJ and Phyton (version 3.7). Statistical significance was calculated with Student's *t*-test and data represent mean±s.e.m. Statistical analysis of MS data was performed with Perseus.

Acknowledgements

We would like to thank Vladimir Rogov, Henrick Riemenschneider, Georg Werner and all members of the Behrends lab for reagents, advice and critical discussion.

Competing interests

The authors declare no competing or financial interests.

Author contributions

Conceptualization: F.E., C.B.; Methodology: F.E., S.P., M.D.S., M.K., C.B.; Validation: F.E., S.P., M.D.S.; Formal analysis: F.E.; Investigation: F.E., S.P., M.D.S.; Resources: F.E.; Data curation: F.E., S.P., M.D.S.; Writing - original draft: F.E., C.B.; Writing - review & editing: F.E., M.K., C.B.; Visualization: F.E., S.P., M.D.S., C.B.; Supervision: S.W., H.F., C.B.; Project administration: C.B.; Funding acquisition: S.W., H.F., C.B.

Funding

This work was supported by the Deutsche Forschungsgemeinschaft (German Research Foundation) within the framework of the Munich Cluster for Systems Neurology (EXC2145 - ID 390857198), the Collaborative Research Center 1177 (ID 259130777) and the project grant BE 4685/2-1. Hesso Farhan was supported by grants from the Norwegian Cancer Society (Kreftforeningen; 182815, 208015), from the Norwegian Research Council (Norges Forskningsråd; 262717) and from the Rakel go Otto Kr. Bruun legat. A Cancer Research UK Career Development Fellowship to S.W. (C20685/A12825) funded this work. M.D.S. was also funded by a Biotechnology and Biological Sciences Research Council (BBSRC) grant to S.W. (BB/N000315/1).

Data availability

The mass spectrometry proteomics data have been deposited to the ProteomeXchange Consortium (<http://proteomecentral.proteomexchange.org>) via the PRIDE partner repository with the dataset identifier PXD016734.

Supplementary information

Supplementary information available online at <https://jcs.biologists.org/lookup/doi/10.1242/jcs.243477.supplemental>

Peer review history

The peer review history is available online at <https://jcs.biologists.org/lookup/doi/10.1242/jcs.243477.reviewer-comments.pdf>

References

- Bai, H., Inoue, J., Kawano, T. and Inazawa, J. (2012). A transcriptional variant of the LC3A gene is involved in autophagy and frequently inactivated in human cancers. *Oncogene* **31**, 4397-4408. doi:10.1038/ncr.2011.613
- Baisamy, L., Cavin, S., Jurisch, N. and Diviani, D. (2009). The ubiquitin-like protein LC3 regulates the Rho-GEF activity of AKAP-Lbc. *J. Biol. Chem.* **284**, 28232-28242. doi:10.1074/jbc.M109.054668
- Behrends, C., Sowa, M. E., Gygi, S. P. and Harper, J. W. (2010). Network organization of the human autophagy system. *Nature* **466**, 68-76. doi:10.1038/nature09204
- Brasaemle, D. L., Dolios, G., Shapiro, L. and Wang, R. (2004). Proteomic analysis of proteins associated with lipid droplets of basal and lipolytically stimulated 3T3-L1 adipocytes. *J. Biol. Chem.* **279**, 46835-46842. doi:10.1074/jbc.M409340200
- Cai, Y., Pi, W., Sivaprakasam, S., Zhu, X., Zhang, M., Chen, J., Makala, L., Lu, C., Wu, J., Teng, Y. et al. (2015). UFBP1, a key component of the Ufm1 conjugation system, is essential for ufmylation-mediated regulation of erythroid development. *PLoS Genet.* **11**, e1005643. doi:10.1371/journal.pgen.1005643
- Culley, S., Tosheva, K. L., Matos Pereira, P. and Henriques, R. (2018). SRRF: Universal live-cell super-resolution microscopy. *Int. J. Biochem. Cell Biol.* **101**, 74-79. doi:10.1016/j.biocel.2018.05.014
- Dejesus, R., Moretti, F., Mcallister, G., Wang, Z., Bergman, P., Liu, S., Frias, E., Alford, J., Reece-Hoyes, J. S., Lindeman, A. et al. (2016). Functional CRISPR screening identifies the ufmylation pathway as a regulator of SQSTM1/p62. *eLife* **5**, e17290. doi:10.7554/eLife.17290
- Dikic, I. and Elazar, Z. (2018). Mechanism and medical implications of mammalian autophagy. *Nat. Rev. Mol. Cell Biol.* **19**, 349-364. doi:10.1038/s41580-018-0003-4
- Ewing, R. M., Chu, P., Elisma, F., Li, H., Taylor, P., Climie, S., Mcbroom-Cerajewski, L., Robinson, M. D., O'connor, L., Li, M. et al. (2007). Large-scale mapping of human protein-protein interactions by mass spectrometry. *Mol. Syst. Biol.* **3**, 89. doi:10.1038/msb4100134
- Fujimoto, Y., Itabe, H., Sakai, J., Makita, M., Noda, J., Mori, M., Higashi, Y., Kojima, S. and Takano, T. (2004). Identification of major proteins in the lipid droplet-enriched fraction isolated from the human hepatocyte cell line HuH7. *Biochim. Biophys. Acta* **1644**, 47-59. doi:10.1016/j.bbamcr.2003.10.018
- Fujimoto, Y., Itabe, H., Kinoshita, T., Homma, K. J., Onoduka, J., Mori, M., Yamaguchi, S., Makita, M., Higashi, Y., Yamashita, A. et al. (2007). Involvement of ACSL in local synthesis of neutral lipids in cytoplasmic lipid droplets in human hepatocyte HuH7. *J. Lipid Res.* **48**, 1280-1292. doi:10.1194/jlr.M700050-JLR200
- Genau, H. M., Huber, J., Baschieri, F., Akutsu, M., Dötsch, V., Farhan, H., Rogov, V. and Behrends, C. (2015). CUL3-KBTBD6/KBTBD7 ubiquitin ligase cooperates with GABARAP proteins to spatially restrict TIAM1-RAC1 signaling. *Mol. Cell* **57**, 995-1010. doi:10.1016/j.molcel.2014.12.040
- Gerakis, Y., Quintero, M., Li, H. and Hetz, C. (2019). The UFMylation system in proteostasis and beyond. *Trends Cell Biol.* **29**, 974-986. doi:10.1016/j.tcb.2019.09.005
- Habisov, S., Huber, J., Ichimura, Y., Akutsu, M., Rogova, N., Loehr, F., Mcewan, D. G., Johansen, T., Dikic, I., Doetsch, V. et al. (2016). Structural and functional analysis of a novel interaction motif within UFM1-activating enzyme 5 (UBA5) required for binding to ubiquitin-like proteins and ufmylation. *J. Biol. Chem.* **291**, 9025-9041. doi:10.1074/jbc.M116.715474
- Henne, W. M., Reese, M. L. and Goodman, J. M. (2018). The assembly of lipid droplets and their roles in challenged cells. *EMBO J.* **37**, e98947. doi:10.15252/embo.201898947
- Huber, J., Obata, M., Gruber, J., Akutsu, M., Löhr, F., Rogova, N., Güntert, P., Dikic, I., Kirkin, V., Komatsu, M. et al. (2019). An atypical LIR motif within UBA5 (ubiquitin like modifier activating enzyme 5) interacts with GABARAP proteins and mediates membrane localization of UBA5. *Autophagy* **16**, 256-270. doi:10.1080/15548627.2019.1606637
- Ingelmo-Torres, M., González-Moreno, E., Kassan, A., Hanzal-Bayer, M., Tebar, F., Herms, A., Grewal, T., Hancock, J. F., Enrich, C., Bosch, M. et al. (2009). Hydrophobic and basic domains target proteins to lipid droplets. *Traffic* **10**, 1785-1801. doi:10.1111/j.1600-0854.2009.00994.x
- Kalvari, I., Tsompanis, S., Mulakkal, N. C., Osgood, R., Johansen, T., Nezis, I. P. and Promponas, V. J. (2014). iLIR: a web resource for prediction of Atg8-family interacting proteins. *Autophagy* **10**, 913-925. doi:10.4161/auto.28260
- Karagöz, G. E., Acosta-Alvear, D. and Walter, P. (2019). The unfolded protein response: detecting and responding to fluctuations in the protein-folding capacity of the endoplasmic reticulum. *Cold Spring Harb. Perspect. Biol.* **11**, a033886. doi:10.1101/cshperspect.a033886
- Kassan, A., Herms, A., Fernández-Vidal, A., Bosch, M., Schieber, N. L., Reddy, B. J. N., Fajardo, A., Gelabert-Baldrich, M., Tebar, F., Enrich, C. et al. (2013). Acyl-CoA synthetase 3 promotes lipid droplet biogenesis in ER microdomains. *J. Cell Biol.* **203**, 985-1001. doi:10.1083/jcb.201305142
- Kaulich, M. and Dowdy, S. F. (2015). Combining CRISPR/Cas9 and rAAV templates for efficient gene editing. *Nucleic Acid Ther.* **25**, 287-296. doi:10.1089/nat.2015.0545
- Kelleher, D. J., Kreibich, G. and Gilmore, R. (1992). Oligosaccharyltransferase activity is associated with a protein complex composed of ribophorins I and II and a 48 kd protein. *Cell* **69**, 55-65. doi:10.1016/0092-8674(92)90118-V
- Kimura, H., Arasaki, K., Ohsaki, Y., Fujimoto, T., Ohtomo, T., Yamada, J. and Tagaya, M. (2018). Syntaxin 17 promotes lipid droplet formation by regulating the distribution of acyl-CoA synthetase 3. *J. Lipid Res.* **59**, 805-819. doi:10.1194/jlr.M081679
- Kirkin, V. and Rogov, V. V. (2019). A diversity of selective autophagy receptors determines the specificity of the autophagy pathway. *Mol. Cell* **76**, 268-285. doi:10.1016/j.molcel.2019.09.005
- Komatsu, M., Chiba, T., Tatsumi, K., Iemura, S.-I., Tanida, I., Okazaki, N., Ueno, T., Kominami, E., Natsume, T. and Tanaka, K. (2004). A novel protein-conjugating system for Ufm1, a ubiquitin-fold modifier. *EMBO J.* **23**, 1977-1986. doi:10.1038/sj.emboj.7600205
- Le Guerroué, F., Eck, F., Jung, J., Starzetz, T., Mittelbronn, M., Kaulich, M. and Behrends, C. (2017). Autophagosomal content profiling reveals an LC3C-dependent piecemeal mitophagy pathway. *Mol. Cell* **68**, 786-796.e6. doi:10.1016/j.molcel.2017.10.029
- Legesse-Miller, A., Sagiv, Y., Porat, A. and Elazar, Z. (1998). Isolation and characterization of a novel low molecular weight protein involved in intra-Golgi traffic. *J. Biol. Chem.* **273**, 3105-3109. doi:10.1074/jbc.273.5.3105

- Leil, T. A., Chen, Z.-W., Chang, C.-S. and Olsen, R. W. (2004). GABAA receptor-associated protein traffics GABAA receptors to the plasma membrane in neurons. *J. Neurosci.* **24**, 11429–11438. doi:10.1523/JNEUROSCI.3355-04.2004
- Lemaire, K., Moura, R. F., Granvik, M., Igoillo-Esteve, M., Hohmeier, H. E., Hendrickx, N., Newgard, C. B., Waelkens, E., Cnop, M. and Schuit, F. (2011). Ubiquitin fold modifier 1 (UFM1) and its target UFBP1 protect pancreatic beta cells from ER stress-induced apoptosis. *PLoS ONE* **6**, e18517. doi:10.1371/journal.pone.0018517
- Liang, J. R., Lingeman, E., Ahmed, S. and Corn, J. E. (2018). Atlantins remodel the endoplasmic reticulum for selective autophagy. *J. Cell Biol.* **217**, 3354–3367. doi:10.1083/jcb.201804185
- Liang, J. R., Lingeman, E., Luong, T., Ahmed, S., Muhar, M., Nguyen, T., Olzmann, J. A. and Corn, J. E. (2020). A genome-wide ER-phagy screen highlights key roles of mitochondrial metabolism and ER-resident UFMylation. *Cell*. **180**, 1160–1177.e20. doi:10.1016/j.cell.2020.02.017
- Liu, J., Wang, Y., Song, L., Zeng, L., Yi, W., Liu, T., Chen, H., Wang, M., Ju, Z. and Cong, Y.-S. (2017). A critical role of DDRGK1 in endoplasmic reticulum homeostasis via regulation of IRE1alpha stability. *Nat. Commun.* **8**, 14186. doi:10.1038/ncomms14186
- Marshall, R. S. and Vierstra, R. D. (2019). Dynamic regulation of the 26S proteasome: from synthesis to degradation. *Front. Mol. Biosci.* **6**, 40. doi:10.3389/fmolb.2019.00040
- Marshall, R. S., Li, F., Gemperline, D. C., Book, A. J. and Vierstra, R. D. (2015). Autophagic degradation of the 26S proteasome is mediated by the dual ATG8/ubiquitin receptor RPN10 in Arabidopsis. *Mol. Cell* **58**, 1053–1066. doi:10.1016/j.molcel.2015.04.023
- Matic, I., Schimmel, J., Hendriks, I. A., Van Santen, M. A., Van De Rijke, F., Van Dam, H., Gnad, F., Mann, M. and Vertegaal, A. C. O. (2010). Site-specific identification of SUMO-2 targets in cells reveals an inverted SUMOylation motif and a hydrophobic cluster SUMOylation motif. *Mol. Cell* **39**, 641–652. doi:10.1016/j.molcel.2010.07.026
- Mizushima, N., Yoshimori, T. and Ohsumi, Y. (2011). The role of Atg proteins in autophagosome formation. *Annu. Rev. Cell Dev. Biol.* **27**, 107–132. doi:10.1146/annurev-cellbio-092910-154005
- Müller, J. M., Shorter, J., Newman, R., Deinhardt, K., Sagiv, Y., Elazar, Z., Warren, G. and Shima, D. T. (2002). Sequential SNARE disassembly and GATE-16-GOS-28 complex assembly mediated by distinct NSF activities drives Golgi membrane fusion. *J. Cell Biol.* **157**, 1161–1173. doi:10.1083/jcb.200202082
- Nguyen, T. N., Padman, B. S., Usher, J., Oorschot, V., Ramm, G. and Lazarou, M. (2016). Atg8 family LC3/GABARAP proteins are crucial for autophagosome-lysosome fusion but not autophagosome formation during PINK1/Parkin mitophagy and starvation. *J. Cell Biol.* **215**, 857–874. doi:10.1083/jcb.201607039
- Noda, N. N., Kumeta, H., Nakatogawa, H., Satoo, K., Adachi, W., Ishii, J., Fujioka, Y., Ohsumi, Y. and Inagaki, F. (2008). Structural basis of target recognition by Atg8/LC3 during selective autophagy. *Genes Cells* **13**, 1211–1218. doi:10.1111/j.1365-2443.2008.01238.x
- Pankiv, S., Clausen, T. H., Lamark, T., Brech, A., Bruun, J.-A., Outzen, H., Øvervatn, A., Bjørkøy, G. and Johansen, T. (2007). p62/SQSTM1 binds directly to Atg8/LC3 to facilitate degradation of ubiquitinated protein aggregates by autophagy. *J. Biol. Chem.* **282**, 24131–24145. doi:10.1074/jbc.M702824200
- Popovic, D., Akutsu, M., Novak, I., Harper, J. W., Behrends, C. and Dikic, I. (2012). Rab GTPase-activating proteins in autophagy: regulation of endocytic and autophagy pathways by direct binding to human ATG8 modifiers. *Mol. Cell Biol.* **32**, 1733–1744. doi:10.1128/MCB.06717-11
- Poppelreuther, M., Rudolph, B., Du, C., Großmann, R., Becker, M., Thiele, C., Eehalt, R. and Füllekrug, J. (2012). The N-terminal region of acyl-CoA synthetase 3 is essential for both the localization on lipid droplets and the function in fatty acid uptake. *J. Lipid Res.* **53**, 888–900. doi:10.1194/jlr.M024562
- Rogov, V., Dötsch, V., Johansen, T. and Kirkin, V. (2014). Interactions between autophagy receptors and ubiquitin-like proteins form the molecular basis for selective autophagy. *Mol. Cell* **53**, 167–178. doi:10.1016/j.molcel.2013.12.014
- Rolland, T., Tasan, M., Charlotiaux, B., Pevzner, S. J., Zhong, Q., Sahni, N., Yi, S., Lemmens, I., Fontanillo, C., Mosca, R. et al. (2014). A proteome-scale map of the human interactome network. *Cell* **159**, 1212–1226. doi:10.1016/j.cell.2014.10.050
- Schaaf, M. B. E., Keulers, T. G., Vooijs, M. A. and Rouschop, K. M. A. (2016). LC3/GABARAP family proteins: autophagy-(un)related functions. *FASEB J.* **30**, 3961–3978. doi:10.1096/fj.201600698R
- Shpilka, T., Weidberg, H., Pietrokovski, S. and Elazar, Z. (2011). Atg8: an autophagy-related ubiquitin-like protein family. *Genome Biol.* **12**, 226. doi:10.1186/gb-2011-12-7-226
- Slobodkin, M. R. and Elazar, Z. (2013). The Atg8 family: multifunctional ubiquitin-like key regulators of autophagy. *Essays Biochem.* **55**, 51–64. doi:10.1042/bse0550051
- Soupe, E. and Kuypers, F. A. (2008). Mammalian long-chain acyl-CoA synthetases. *Exp. Biol. Med. (Maywood)* **233**, 507–521. doi:10.3181/0710-MR-287
- Stadel, D., Millarte, V., Tillmann, K. D., Huber, J., Tamin-Yecheskel, B.-C., Akutsu, M., Demishtein, A., Ben-Zeev, B., Anikster, Y., Perez, F. et al. (2015). TECPR2 cooperates with LC3C to regulate COPII-dependent ER export. *Mol. Cell* **60**, 89–104. doi:10.1016/j.molcel.2015.09.010
- Stolz, A., Ernst, A. and Dikic, I. (2014). Cargo recognition and trafficking in selective autophagy. *Nat. Cell Biol.* **16**, 495–501. doi:10.1038/ncb2979
- Stolz, A., Putyrski, M., Kutle, I., Huber, J., Wang, C., Major, V., Sidhu, S. S., Youle, R. J., Rogov, V. V., Dötsch, V. et al. (2017). Fluorescence-based ATG 8 sensors monitor localization and function of LC 3/GABARAP proteins. *EMBO J.* **36**, 549–564. doi:10.15252/embj.201695063
- Tatsumi, K., Sou, Y.-S., Tada, N., Nakamura, E., Iemura, S.-I., Natsume, T., Kang, S. H., Chung, C. H., Kasahara, M., Kominami, E. et al. (2010). A novel type of E3 ligase for the Ufm1 conjugation system. *J. Biol. Chem.* **285**, 5417–5427. doi:10.1074/jbc.M109.036814
- Tatsumi, K., Yamamoto-Mukai, H., Shimizu, R., Waguri, S., Sou, Y.-S., Sakamoto, A., Taya, C., Shitara, H., Hara, T., Chung, C. H. et al. (2011). The Ufm1-activating enzyme Uba5 is indispensable for erythroid differentiation in mice. *Nat. Commun.* **2**, 181. doi:10.1038/ncomms1182
- Walczak, C. P., Leto, D. E., Zhang, L., Riepe, C., Muller, R. Y., Darosa, P. A., Ingolia, N. T., Elias, J. E. and Kopito, R. R. (2019). Ribosomal protein RPL26 is the principal target of UFMylation. *Proc. Natl. Acad. Sci. USA* **116**, 1299–1308. doi:10.1073/pnas.1816202116
- Wang, H., Bedford, F. K., Brandon, N. J., Moss, S. J. and Olsen, R. W. (1999). GABA(A)-receptor-associated protein links GABA(A) receptors and the cytoskeleton. *Nature* **397**, 69–72. doi:10.1038/16264
- Weidberg, H., Shpilka, T., Shvets, E., Abada, A., Shimron, F. and Elazar, Z. (2011). LC3 and GATE-16 N termini mediate membrane fusion processes required for autophagosome biogenesis. *Dev. Cell* **20**, 444–454. doi:10.1016/j.devcel.2011.02.006
- Wu, J., Lei, G., Mei, M., Tang, Y. and Li, H. (2010). A novel C53/LZAP-interacting protein regulates stability of C53/LZAP and DDRGK domain-containing Protein 1 (DDRGK1) and modulates NF-kappaB signaling. *J. Biol. Chem.* **285**, 15126–15136. doi:10.1074/jbc.M110.110619
- Xie, Z., Nair, U. and Klionsky, D. J. (2008). Atg8 controls phagophore expansion during autophagosome formation. *Mol. Biol. Cell* **19**, 3290–3298. doi:10.1091/mbc.e07-12-1292
- Yoo, H. M., Kang, S. H., Kim, J. Y., Lee, J. E., Seong, M. W., Lee, S. W., Ka, S. H., Sou, Y.-S., Komatsu, M., Tanaka, K. et al. (2014). Modification of ASC1 by UFM1 is crucial for ERalpha transactivation and breast cancer development. *Mol. Cell* **56**, 261–274. doi:10.1016/j.molcel.2014.08.007
- Zhang, Y., Zhang, M., Wu, J., Lei, G. and Li, H. (2012). Transcriptional regulation of the Ufm1 conjugation system in response to disturbance of the endoplasmic reticulum homeostasis and inhibition of vesicle trafficking. *PLoS ONE* **7**, e48587. doi:10.1371/journal.pone.0048587
- Zhang, M., Zhu, X., Zhang, Y., Cai, Y., Chen, J., Sivaprakasam, S., Gurav, A., Pi, W., Makala, L., Wu, J. et al. (2015). RCAD/Ufm1, a Ufm1 E3 ligase, is essential for hematopoietic stem cell function and murine hematopoiesis. *Cell Death Differ.* **22**, 1922–1934. doi:10.1038/cdd.2015.51
- Zhu, H., Bhatt, B., Sivaprakasam, S., Cai, Y., Liu, S., Kodeboyina, S. K., Patel, N., Savage, N. M., Sharma, A., Kaufman, R. J. et al. (2019). Ufbp1 promotes plasma cell development and ER expansion by modulating distinct branches of UPR. *Nat. Commun.* **10**, 1084. doi:10.1038/s41467-019-08908-5